

Highly modular piano-stool N-heterocyclic carbene iron complexes: impact of ligand variation on hydrosilylation activity

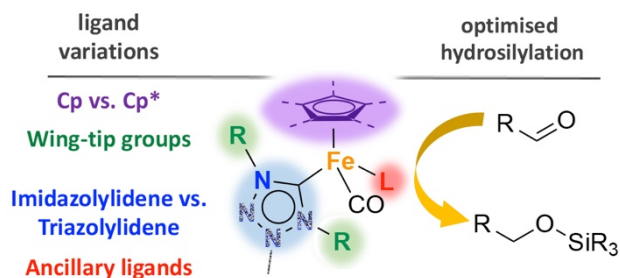
Pamela V. S. Nylund,[†] Nathalie C. Ségaud[†] and Martin Albrecht ^{*,†}

[†] Department of Chemistry & Biochemistry, University of Bern, Freiestrasse 3, 3012 Bern,
Switzerland

* E-mail address: martin.albrecht@dcb.unibe.ch (M. Albrecht)

ABSTRACT: The piano-stool configuration combined with N-heterocyclic carbene (NHC) ligation constitutes an attractive scaffold for employing iron in catalysis. Here we have expanded this scaffold by installing a Cp* ligand as a strong

electron donor compared to the traditionally used unsubstituted Cp. Moreover, decarboxylation is introduced as a method to prepare these iron(II) NHC complexes, which avoids the isolation of air-sensitive free carbenes. In addition to the Cp/Cp* variation, the complexes have been systematically modulated at the NHC scaffold, the NHC wingtip groups, and the ancillary ligands in order to identify critical factors that govern the catalytic activity of the iron centre in the hydrosilylation of aldehydes. These modulations reveal the importance of steric tailoring and optimization of electron density for high catalytic performance. The data demonstrate a critical role of the NHC scaffold, with triazolylidenes imparting consistently higher activity than imidazolylidenes, and a correlation between catalytic activity and steric rather than electronic factors. Moreover, implementation of steric bulk is strongly dependent on the nature of the NHC and severely limited by the Cp* iron precursor. Best performing catalytic systems reach turnover frequencies TOF_{max} up to 360 h⁻¹ at 60 °C. Mechanistic investigations by ¹H NMR and *in situ* IR spectroscopies indicate a catalyst activation that involves CO release and aldehyde coordination to the [Fe(Cp)(NHC)I] fragment.



INTRODUCTION

Iron is the second most abundant metal in the earth crust, easy to extract and consequently cheap. Additionally, it is biological relevant and known to be nontoxic both to humans and the environment. Despite these facts, iron was for a long time scarce in the catalytic literature compared to some of the more expensive, rare and toxic metals in the periodic system. Application of iron as molecular catalyst has been catching up with other metals over the last 20 years, however, and is now covering a plethora of organic reactions.¹⁻³ Hydrosilylation, one of the fields which has received much attention in iron catalysis during the past decades,⁴⁻⁸ is a versatile methodology for the reduction of a variety of substrates under base-free conditions and without the need for highly reducing conditions as imparted by H₂ pressure.⁸⁻¹⁰ In particular, hydrosilylation of alkenes is industrially important due to the increasing demand for silanes and siloxanes.¹¹

In the past two decades iron complexes have emerged as attractive hydrosilylation catalysts for alkenes in an approach to make industrial hydrosilylation more benign. While these systems normally deploy NN or NNN type ligands,¹²⁻¹⁶ piano-stool iron complexes with N-heterocyclic carbene (NHC) ligands have demonstrated efficiency in the hydrosilylation of carbonyls rather than alkenes under fairly mild conditions.¹⁷⁻²¹ These iron(II) complexes offer an excellent, cheap and non-toxic alternative to systems based on noble metals such as rhodium, palladium and platinum.⁸ The synthesis of NHC iron complexes is traditionally accomplished via the versatile free carbene route.²²⁻²⁵ The need of base and inert conditions however poses limitations, and especially NHCs with small wingtip groups risk rearrangement or decomposition under basic conditions.²⁴⁻²⁶ Here we present a new synthetic method to prepare NHC iron(II) piano-stool complexes. Moreover, we have used this and traditional methods to modularize NHC iron piano-

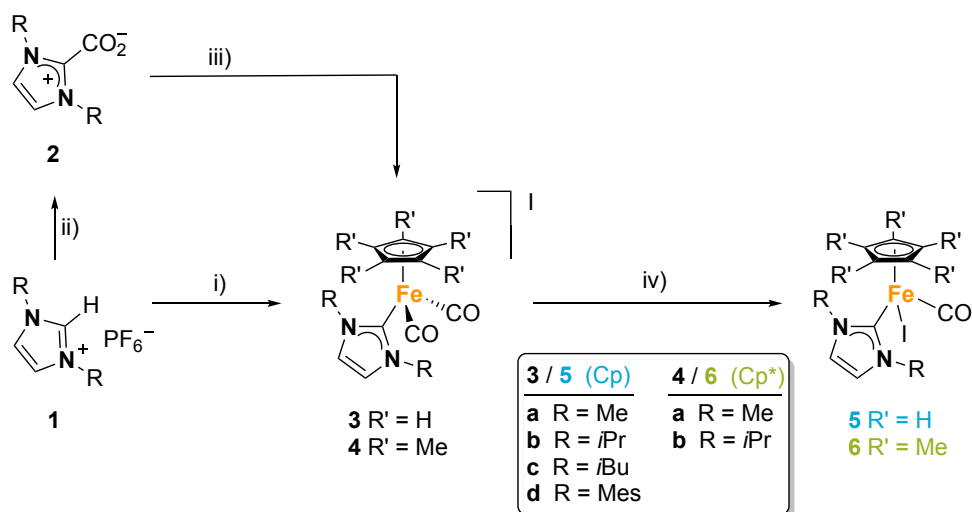
stool complexes to evaluate the effects of variation in the cyclopentadiene (Cp) unit, the NHC scaffold and the wingtip groups on catalytic hydrosilylation activity, demonstrating the importance of considering even slightly different catalysts depending on the substrate.

RESULTS AND DISCUSSION

Synthesis of imidazole-derived NHC complexes. The known imidazolylidene iron Cp complexes **3a**, **3b**, **3d**^{22,23,27} and the new complex **3c** were prepared by the established free base route involving the deprotonation of the corresponding imidazolium salts **1a–d** with KO*t*Bu followed by addition of the iron precursor [FeCp(CO)₂I] (Scheme 1).^{22,23} Using the pentamethyl cyclopentadienyl (Cp*) precursor [FeCp*(CO)₂I] instead afforded complexes **4a** and **4b** in good yields. However, the analogous complex from imidazolium salt **1c** with isobutyl wingtip groups did not form, suggesting higher steric congestion imparted by the Cp* ligand as compared to the Cp system. Notably, two- and three-legged piano-stool complexes with mesityl-substituted NHC ligands were successfully prepared by the groups of Tatsumi and Song starting from the CO-free iron precursors [Cp*Fe[N(SiMe₃)₂], [Cp*FeCl(TMEDA)], and [FeCp*(HMDS)] (TMEDA = Me₂NCH₂CH₂NMe₂, HMDS = N(SiMe₃)₂).^{28–31}

Iron NHC complexes are generally prepared from the air and moisture sensitive free carbene, which requires inert conditions.^{32–34} Here we demonstrate that the decarboxylation method offers an attractive alternative for the synthesis of these iron complexes. While this strategy has previously been applied predominantly for platinum group metals,³⁵ its application to first-row transition metals is much rarer and mostly involves copper, and has never been applied to iron(II) precursors so far.^{36–40} Reaction of the imidazolium carboxylate **2a** with [FeCpI(CO)₂] induced release of CO₂ and afforded the known complex **3a** in similar yields as via the deprotonation route

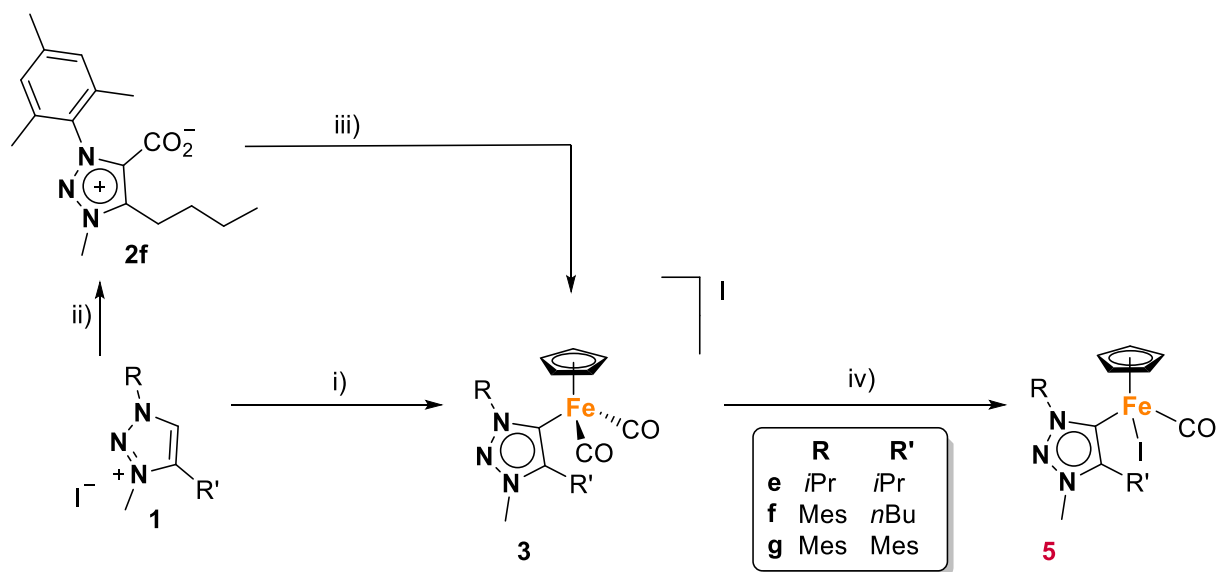
(43% vs 58%, Scheme 1).²³ Attractively, the metallation via decarboxylation proceeds in a distinct step that is not air- or moisture sensitive, and avoids the tedious isolation of the air-sensitive free carbene prior to transfer to the iron precursor. Likewise, the new Cp* complexes **4a** and **4b** were also generated via decarboxylation of the imidazolium carboxylates **2a** and **2b**, respectively.^{35,41}



Scheme 1. Synthesis of iron imidazolylidene complexes. Reagents and conditions: (i) KO*t*Bu, THF, rt, 60 min, then [Cp^(*)Fe(CO)₂I], toluene, rt, 16 h; (ii) KO*t*Bu, THF, rt, 60 min, then CO₂, toluene, rt, 1 h; (iii) [Cp^(*)Fe(CO)₂I], toluene, 80 °C, 16 h; (iv) *hν*, CH₂Cl₂, 16 h.

The formation of the new cationic iron complexes **3c** and **4a,b** was supported in ¹H NMR spectroscopy by the expected relative integral ratio of the ligand signals and those of the Cp or Cp* fragments at 5.31 and 1.83 ± 0.01 ppm, respectively, and by the characteristic Fe–C_{carbene} resonance at δ_C 162.5 ± 10.5 (Fig. S1–S26). UV irradiation in CH₂Cl₂ induced CO release and iodide coordination to form the neutral complexes **5** and **6**. Ligand exchange was indicated by a characteristic color change from yellow to green as well as a diagnostic upfield shift of the Cp resonance in the ¹³C NMR spectra from δ_C ~88 to ~80 in complexes **5** and from ~99 to ~90 in the Cp* complexes **6** as a consequence of the substitution of the π-accepting CO ligand with the

stronger donating iodide (Fig. S27–S38 and Fig S39–S44, respectively). All ^1H and ^{13}C NMR shifts are in the same range as those of related complexes.^{17,19,22}



Scheme 2. Synthesis of iron triazolylidene complexes. Reagents and conditions: (i) KO*t*Bu, THF, rt, 60 min, then [CpFe(CO)₂I], toluene, rt, 16 h; (ii) KO*t*Bu, THF, rt, 60 min then CO₂, toluene, rt, 1 h; (iii) [CpFe(CO)₂I], toluene, 80 °C, 16 h; (iv) *hν*, CH₂Cl₂, 16 h.

Analogous triazolylidene complexes were obtained from the triazolium salts **1e–g**. Formation of previously reported complexes **3f,g** proceeded smoothly via deprotonation with KO*t*Bu,²⁷ and the same methodology was applied to the triazolium salt **1e** to afford the new complex **3e** in moderate yields (Scheme 2). Notably, the iron triazolylidene complex **3f** was also accessible via the decarboxylation route from the new triazolium carboxylate **2f** and [FeCp(CO)₂I] in similar yields as via the free carbene route (39% vs 42%). When irradiated, the cationic triazolylidene complexes **3e–g** transformed into the neutral complexes **5e–g**, which was indicated by a diagnostic colour change from yellow to green as well as spectroscopic changes similar to those described for the imidazolylidene analogues, including an upfield shift of the Cp carbon signals from δ_{C} 88 to 80 ppm as well as a ~20 ppm downfield shift of the Fe–C_{carbene} resonances. All new imidazolylidene

and triazolylidene complexes were stable as solids in ambient atmosphere, but slowly decomposed in solution, indicated macroscopically by a gradual colour change to brown and the formation of a precipitate, and microscopically by considerable broadening of the ^1H NMR signals.

Remarkably, the synthesis of the Cp* analogues of **3e** and **3f** has failed in our hands. Neither the free carbene nor the decarboxylation route afforded the desired complexes. In an effort to increase the reactivity, *in situ* prepared cationic $[\text{FeCp}^*(\text{CO})_2(\text{THF})]\text{OTf}$ was used as iron precursor⁴² together with the free carbene from **1f**, though only paramagnetic products were obtained. In contrast, the triazolium salt **1e** with similar steric implications as the imidazolium salt **1b** gave, after deprotonation and reaction with $[\text{FeCp}^*(\text{CO})_2\text{I}]$, the triazolylidene analogue of complex **4b** as suggested by the correct relative integral ratio of the ligand signals and the Cp–Me groups from a crude sample (Fig. S45). Moreover, irradiation of the crude mixture induced the diagnostic color change to green, however only traces of this complex were isolated, and we failed to develop synthetic methods to obtain this complex in sufficiently high quantities. Nonetheless, these experiments indicate that three-legged piano-stool Fe–Cp* complexes with triazolylidene complexes should, in principle, be accessible. Notably, Song reported in 2020 a two-legged piano-stool Fe–Cp* complex with a triazolylidene ligand.³¹

Structural analyses

Solid state X-ray crystal structures of representative examples of complexes **3–6** confirmed the piano-stool geometry and revealed bond lengths and angles in the expected range (Fig. 1, Tables 1 and 2).^{22,23,27} The Fe–C_{carbene} bonds and the Fe–Cp distances are only marginally elongated (<0.025 Å) in the Cp* complexes compared to their Cp analogues. Also the relative orientation of

the carbene ligand, determined by the N–C_{carbene}–Fe–C_{pcentroid} dihedral angle θ , does not reveal any significant twists of the carbene in the cationic complexes **3** and **4** ($\theta = 91.7^\circ \pm 1.3^\circ$) except for complex **3f** and **3g** ($\theta = 98.9^\circ$ and 98.4° respectively), which was attributed to steric constraints between the mesityl groups and the Cp protons.³⁴ The differences are more noticeable for the neutral complexes **5** and **6** (θ between 92° and 136°), suggesting a more flexible rotation. This flexibility may be facilitated by the smaller I–Fe–CO bond angle as compared to the CO–Fe–CO bond angle in the cationic analogues.

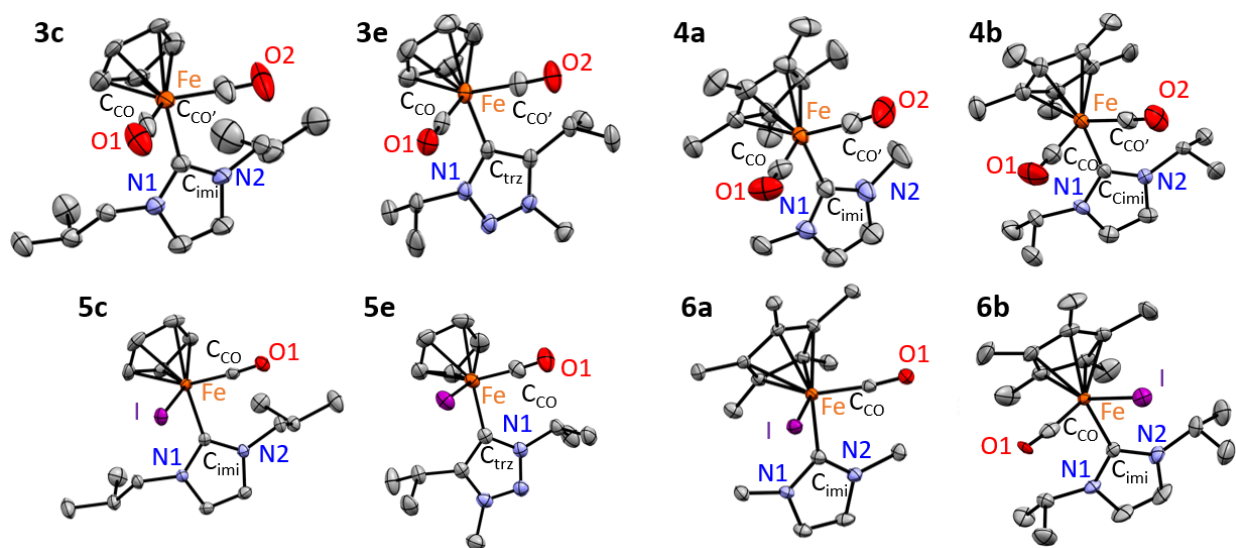


Figure 1. ORTEP representations (50% probability level) of the new cationic complexes **3c,e** and **4a,b** and the neutral analogues **5c,e** and **6a,b**. Hydrogen atoms and noncoordinating anions omitted for clarity and atom labeling adjusted for consistency.

Table 1. Selected bond lengths [\AA] and angles [$^\circ$] for cationic Cp complexes **3** and Cp* complexes **4**.

complex	3a ^a	3b ^a	3c ^b	3e	3f ^a	3g ^a	4a	4b
ligand set	imi/Cp	imi/Cp	imi/Cp	trz/Cp	trz/Cp	trz/Cp	imi/Cp*	imi/Cp*
Fe–C _{imi/trz}	1.969(6)	1.970(3)	1.965(6)	1.976(3)	1.974(3)	2.010(6)	1.979(4)	1.995(6)
Fe–C _{CO}	1.777(5)	1.774(4)	1.769(9)	1.775(3)	1.765(4)	1.774(7)	1.762(5)	1.759(8)
Fe–C _{CO'}	1.777(5)	1.780(3)	1.768(9)	1.767(3)	1.773(4)	1.767(6)	1.767(5)	1.772(8)
Fe–C _{centroid}	1.731	1.716	1.752	1.718	1.724	1.727	1.743	1.738

C _{CO} -Fe-C _{imi/trz}	95.05(19)	94.2(1)	93.1(3)	94.07(12)	98.82(14)	99.26(3)	94.48(19)	93.6(3)
C _{CO} -Fe-C _{imi/trz}	95.05(19)	94.4(2)	93.7(3)	92.58(12)	91.17(14)	97.54(6)	94.7(2)	95.2(3)
C _{CO} -Fe-C _{CO}	93.4(3)	92.8(2)	90.5(4)	92.36(13)	92.24(17)	94.89(7)	93.1(2)	91.5(4)
C _{trz} -Fe-C _{pcentroid}	120.82	122.2	121.00	122.13	120.46	121.4(7)	122.92	123.50
N-C _{trz} -Fe-C _{pcentroid}	91.40	91.86	92.89	90.97	98.94	98.38	90.75	90.40

^a Values obtained from ref. 23 (**3a** and **3b**) and ref 27 (**3f** and **3g**). ^b Mixed occupation of anion site with I (82.3%) or PF₆ (17.7%). imi = imidazolylidene, trz = triazolylidene.

Table 2. Selected bond lengths [Å] and angles [°] for neutral Cp complexes **5** and Cp* complexes **6**.

complex ligand set	5a ^a imi/Cp	5b ^a imi/Cp	5c imi/Cp	5d ^a imi/Cp	5e trz/Cp	5g ^a trz/Cp	6a imi/Cp*	6b imi/Cp*
Fe-C _{NHC}	1.964(3)	1.972(5)	1.9652 (19)	1.980(5)	1.990(4)	1.974(3)	1.970(3)	1.988(4)
Fe-C _{CO}	1.749(3)	1.743(6)	1.7470 (19)	1.641(9)	1.777(5)	1.747(3)	1.744(3)	1.736(5)
Fe-I	2.6548(3)	2.6597(8)	2.6428 (3)	2.6445(8)	2.6813(6)	2.6391(4)	2.6582(4)	2.6452(6)
Fe-C _{centroid}	1.730	1.726	1.727	1.742	1.744	1.722	1.743	1.743
C _{CO} -Fe-C _{NHC}	97.00(11)	95.2(3)	95.32(8)	101.2(5)	96.99(18)	99.48(13)	97.89(13)	97.80(17)
C _{NHC} -Fe-I	92.35(7)	96.88(15)	92.98 (5)	93.12	93.02(10)	92.16(7)	92.41(8)	95.46(11)
C _{CO} -Fe-I	88.96(9)	85.3(2)	85.35(6)	86.5(3)	86.53(13)	89.91(10)	87.91(9)	86.75(15)
C _{NHC} -Fe-C _{pcentroid}	123.43	120.54	124.52	126.22	121.69	125.15	122.86	122.95
N-C _{NHC} -Fe-C _{pcentroid}	107.06	93.88	97.73	134.52	126.89	135.78	105.43	91.98

^aValues obtained from ref. 23 (**5a** and **5b**), 22 (**5d**) and 27 (**5g**).

The steric implications of the Cp*-ligand was investigated by inspecting the shortest distance to NHC wingtip protons in each structure (Table S1). For the Cp complexes **3** and **5**, the closest Cp-H...H_{NHC} contacts were all between 2.25–2.74 Å, with **3b** displaying the shortest distance and **3c** the longest. The Cp* complexes featured slightly shorter Cp-CH₃...H_{NHC} distances (2.12–2.35 Å). Comparison of Cp and Cp* complexes with identical NHC ligand revealed a 0.26 ± 0.12 Å closer contact in the Cp* complex. Close Cp-H...H_{NHC} contacts were also identified in solution by Nuclear Overhauser effects (NOEs) between the Cp* protons and the HC_{IPr} protons for **6b**. Notably, no such NOE signals were detected in **5b** with the same NHC ligand yet a less bulky Cp instead of Cp*. Interactions with the Cp ligand only became apparent when NHCs with bulkier

wingtip groups are coordinated. For example, the Cp protons in complex **5f** showed a NOE with both the mesityl-CH₃ and the N-CH₂ unit (Fig. S51–S53). These results suggest that steric hindrance of the Cp* ligand imposes more steric hindrance for bulky NHC ligands to coordinate to the iron centre and rationalize the failure in preparing the Cp* analogue of complex **3f** (*vide supra*).

While the Cp complex **5a** with small Me wingtip groups on the NHC ligand is fluxional due to rotation about the Fe–C_{NHC} bond and requires low temperature (–20 °C) to reach decoalescence of the resonances in the ¹H NMR spectrum ($\Delta G^\ddagger \sim 59 \text{ kJ mol}^{-1}$),²³ the analogous Cp* complex **6a** is more rigid and reveals a slow exchange limit spectrum with two non-equivalent N-CH₃ resonances at $\delta_{\text{H}} = 4.04$ and 3.86 respectively (Fig. S39).⁴³ In contrast, the signals from the *i*Bu wingtip groups of complex **5c** were broad at room temperature, though they sharpened upon cooling to –20 °C (Fig. S28, Table S2). From the coalescence temperature of these signals ($T_{\text{coal}} = 298 \text{ K}$) and the C_{imi}–H resonance frequencies, a free energy of activation $\Delta G^\ddagger = 58.0 \pm 1.0 \text{ kJ mol}^{-1}$ was calculated for **5c**. Complex **5e** shows two rotamers in the ¹H NMR spectrum at –25 °C, with a free energy of activation $\Delta G^\ddagger = 60.5 \pm 1.0 \text{ kJ mol}^{-1}$ (Fig S32, Table S3). This higher energy compared to **5c** is commensurate with the larger steric demand of the wingtip groups in **5e**.

Donor properties of the ligand sets

To determine the combined electron donor properties of the NHC ligand and the Cp^(*) moiety, the complexes were analysed electrochemically and by IR spectroscopy. IR analysis revealed the characteristic symmetric and asymmetric bands $\nu_{\text{s}} = 2037 \pm 12 \text{ cm}^{-1}$ and $\nu_{\text{as}} = 1990 \pm 13 \text{ cm}^{-1}$ for the cationic bis-carbonyl complexes **3** and **4** and a single absorption in the 1910–1935 cm^{–1} range for the neutral mono-carbonyl complexes **5** and **6** (Table 3). Triazole-derived NHCs induce

generally a 6 ± 1 cm^{-1} lower energy vibration than imidazolyliidenes (*cf* **5b** vs **5e**, and **5d** vs **5g**), in line with the increased electron donor properties of triazolyliidenes.⁴⁴ Wingtip group modification had minor implications for both imidazole- and triazole-derived carbenes in the cationic systems, yet induced some variation in the neutral complexes ($\Delta\nu_{\text{max}} = 7$ cm^{-1} , *cf* **5f** vs **5e**, and **6a** vs **6b**). The most substantial shift was noted upon replacing the Cp ligand for Cp* ($\Delta\nu = 22\pm 4$ cm^{-1}), indicating a major effect of the stronger electron donating Cp* ligand (*cf* **3a,b** vs **4a,b**, and **5a,b** vs **6a,b**).

Table 3. Vibrational and Electrochemical Data for Cationic and Neutral Fe(II) Complexes **3–6**

complex	NHC	wingtip	Cp ^(*)	$\nu_{\text{CO}}/\text{cm}^{-1}$ ^a	$E_{1/2}, (\Delta E) / \text{V}$ ^b
3a	imi	Me	Cp	2048, 2000	
3b	imi	<i>i</i> Pr	Cp	2050, 2003	
3c	imi	<i>i</i> Bu	Cp	2049, 2002	
3d ^c	imi	Mes	Cp	2050, 2006	
3e	trz	<i>i</i> Pr	Cp	2042, 1996	
3f ^d	trz	Mes, <i>n</i> bu	Cp	2041, 1994	
3g ^d	trz	Mes, Mes	Cp	2047, 2002	
3e	trz	<i>i</i> Pr	Cp	2042, 1996	
3f ^d	trz	Mes, <i>n</i> bu	Cp	2041, 1994	
4a	imi	Me	Cp*	2027, 1977	
4b	imi	<i>i</i> Pr	Cp*	2024, 1977	
5a	imi	Me	Cp	1932	+0.45 (0.10)
5b	imi	<i>i</i> Pr	Cp	1934	+0.41 (0.09)
5c	imi	<i>i</i> Bu	Cp	1934	+0.48 (0.09)
5d	imi	Mes	Cp	1938	+0.41 (0.09)
5e	trz	<i>i</i> Pr, <i>i</i> Pr	Cp	1928	+0.35 (0.10)
5f	trz	Mes, <i>n</i> bu	Cp	1935	+0.40 (0.10)
5g ^c	trz	Mes, Mes	Cp	1933	+0.34
6a	imi	Me	Cp*	1914	+0.19 (0.10)
6b	imi	<i>i</i> Pr	Cp*	1910	+0.15 (0.09)

^a measured in CH₂Cl₂. ^b Measured in CH₂Cl₂ using 0.1 M [Bu₄N][PF₆] as supporting electrolyte, sweep rate 100 mV s⁻¹, referenced vs SSCE using Fc⁺/Fc as internal standard (E_{1/2} = +0.46 V, ΔE = 0.1), in parenthesis ΔE = E_{pa} – E_{pc}. ^c from ref. 22. ^d from ref. 27.

Further insights into the electronic modulation of these complexes were gained by electrochemical analysis. While the cationic complexes did not show any oxidation process up to 1.4 V vs SSCE, the neutral complexes **5** and **6** feature a reversible oxidation in cyclic voltammetry (CV; Fig. S54). The half-wave potentials shift only slightly by <90 mV upon changing the wingtip group (Table 3). Substituting the imidazolylidene scaffold for a triazolylidene lowered the oxidation potential by 0.065 ± 0.05 V (*cf* **5b,d** vs **5e,5g**), and exchange of Cp for Cp* had again the largest effect and shifted the redox potential by 0.27V (*cf* **5a,b** vs **6a,b**). These data are in good agreement with the trends deduced from IR spectroscopy and indicate that the Cp/Cp* modulation is 2–3 times larger than the swap of the NHC from imidazolylidene to triazolylidene. Wingtip modification is non-linear, and the electron-donating character of secondary alkyl groups is counterbalanced by steric effects, especially with Cp* ligands. According to both analyses, complex **6b** features the most electron rich iron center with decreasing electron-density along the series **6b** > **6a** > **5e** > **5g** > **5f** > **5d** > **5b** > **5a** > **5c**. These effects are displayed in Fig. 2 for representative examples featuring variable wingtip group, NHC scaffold and Cp vs Cp* ligand, respectively.

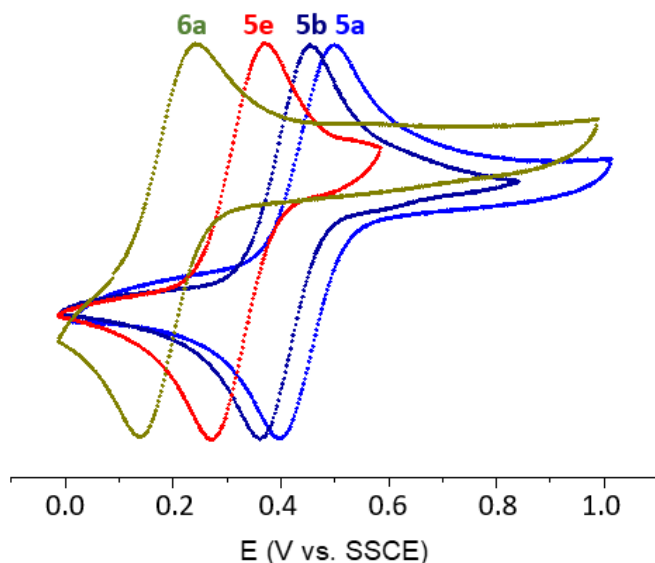


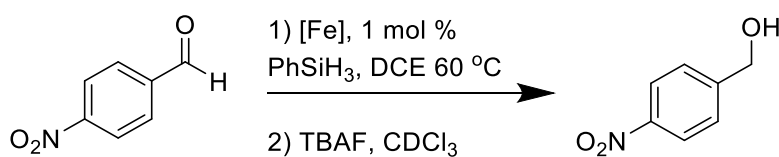
Figure 2. Normalised cyclic voltammograms of representative complexes **5a**, **5b**, **5e** and **6a** measured in CH_2Cl_2 , 0.1 M $[\text{Bu}_4\text{N}]\text{PF}_6$, potential in V vs SSCE and referenced to Fc^+/Fc ($E_{1/2} = +0.46$ V, $\Delta E = 0.1$ V) or decamethyl ferrocene ($E_{1/2} = +0.11$ V, $\Delta E = 0.1$ V), 100 mV s^{-1} sweep rate.

Catalytic hydrosilylation of carbonyl compounds

The impact of the broad electronic tunability of these iron complexes **5** and **6** was evaluated in the reduction of carbonyl compounds via hydrosilylation.^{18,27} 4-Nitrobenzaldehyde was employed as a benchmark substrate and PhSiH_3 as hydrosilylation agent, and yields were calculated after Si–O bond cleavage with Bu_4NF (Table 4). Very distinct time-conversion profiles were observed which indicate a profound influence of the ligand set on the catalytic activity (Fig. 3). Comparison of the catalytic performance revealed some general trends. Firstly, introducing a Cp^* spectator ligand instead of Cp is detrimental to catalytic activity and leads to considerably slower conversion (*cf* complexes **5a** and **6a**, $\text{TOF}_{\text{max}} = 30$ vs 20 h^{-1} , entries 1, 8), though this is less pronounced when the carbene contains *iPr* instead of methyl wingtip groups (**5b** vs **6b**, entries 2, 9). Secondly, replacing the carbene scaffold from imi to trz reduces the reaction time and enhances the catalytic performance considerably (*cf* complexes **5b** and **5e**, $\text{TOF}_{\text{max}} = 50$ vs 160 h^{-1} , entry 2, 5, and

complexes **5d** and **5g**, $\text{TOF}_{\text{max}} = 140$ vs 230 h^{-1} , entries 4, 7), with previously reported complex **5g** as the most active complex in this series.²⁷ And thirdly, wingtip modulations have a marked effect on turnover frequencies and raise from $\text{Me} < i\text{Pr}, i\text{Bu} < \text{Mes}$ for the imi series (entries 1–4) and similarly from $i\text{Pr}, i\text{Pr} < n\text{Bu}, \text{Mes} < \text{Mes}, \text{Mes}$ in the trz series (entries 5–7). The complexes show varying induction times ranging from 10 up to 90 min, suggesting that the active catalyst is formed *in situ*.

Table 4. Hydrosilylation of 4-nitro benzaldehyde by iron(II) complexes **5–6**.^a



entry	[Fe]	conversion (%) ^b	yield (%) ^c	induction (min)	time (h)	TOF_{max} (h^{-1})
1	5a	100	89	90	21	30
2	5b	100	93	<20	2.5	50
3	5c	100	90	<10	3	50
4 ^d	5d	97	n.d.	30	1	140
5	5e	100	99	10	0.83	160
6	5f	100	88	10	0.83	180
7 ^d	5g	99	n.d.	30	1	230
8	6a	100	94	90	21	20
9	6b	100	95	50	3	50
10	[FeCp*(CO) ₂ I]	<2	<2	-	21	-
11	1b	<2	<2	-	21	-

^a General conditions: substrate (0.5 mmol), PhSiH₃ (0.6 mmol), [Fe] complex (5 μmol, 1 mol%), C₆Me₆ as internal standard (50 μmol), 1,2-dichloroethane (DCE; 2.5 mL), 60 °C. ^b Conversion determined by ¹H NMR spectroscopy as an average of at least two runs. ^c Spectroscopic yield after alcohol deprotection. ^d from ref 27.

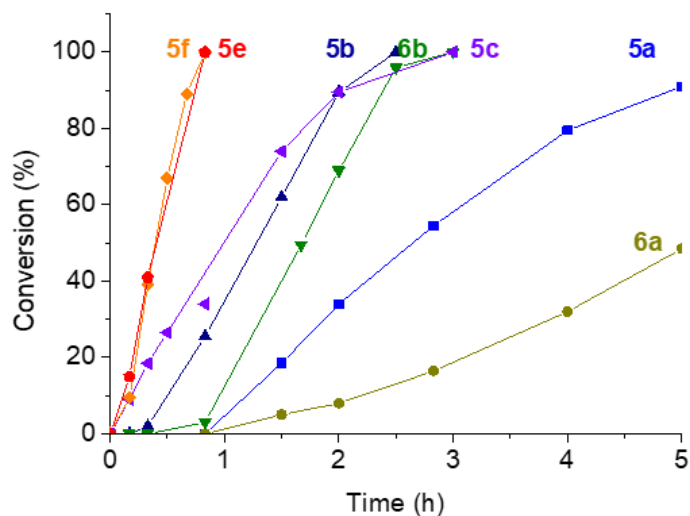


Figure 3. Time-conversion profile of the hydrosilylation of 4-nitrobenzaldehyde by iron(II) complexes 5–6 (conditions as in Table 4).

Notably, there is no clear correlation between the catalytic performance and the redox potential as a proxy for the donor properties of the ligand set (Fig. 4a). While there is a good trend in the Cp series with more donating NHCs increasing the activity, this trend is not confirmed by the imi/Cp* series which should provide much higher activity than observed if the electron density at iron is indeed the decisive factor for catalytic performance.

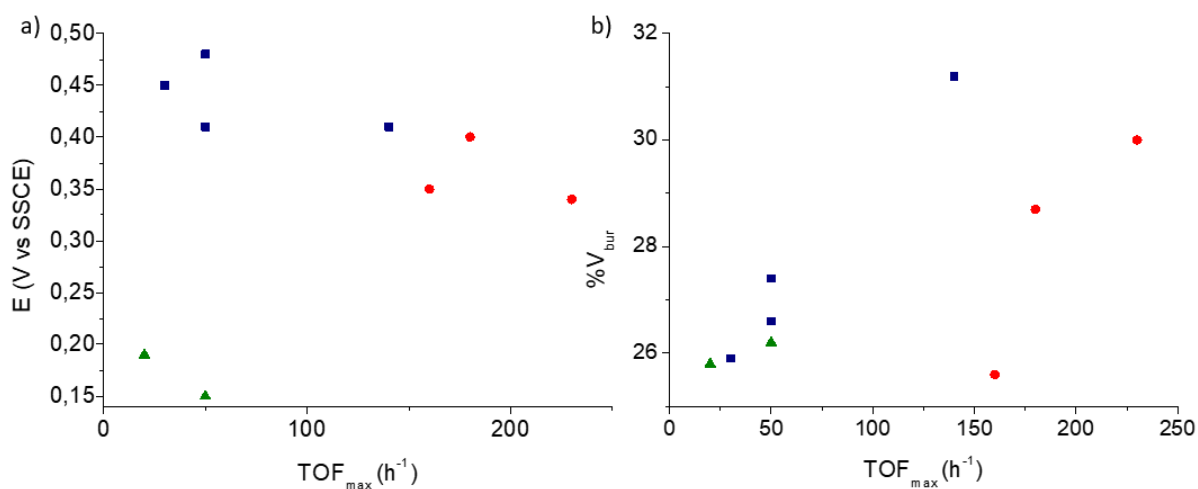


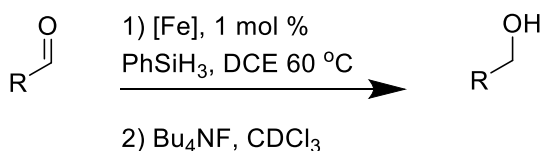
Figure 4. a) Plot of oxidation potentials ($E_{1/2}$) vs TOF_{max} for the catalytic hydrosilylation of 4-nitrobenzaldehyde; b) correlation of buried volume ($\%V_{\text{bur}}$) with TOF_{max} . Color code: imi/Cp ligand set in blue, trz/Cp ligand set in red, imi/Cp* ligand set in green.

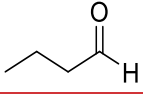
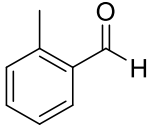
A more stringent trend was revealed when the catalytic activity of the complexes was correlated with the steric influence of the NHC ligand (Fig. 4b) as deduced from the percentage buried volume $\%V_{\text{bur}}$ calculated with the SambVca software (Fig. S55).⁴⁵ Accordingly, even slight increase of the percentage buried volume leads to a higher catalyst performance, with the mesityl-substituted NHCs ($V_{\text{bur}} = 30\text{--}31.2\%$, $\text{TOF}_{\text{max}} = 180\text{--}230 \text{ h}^{-1}$) performing better than the analogues with alkyl wingtip groups ($V_{\text{bur}} = 25.6\text{--}27.4\%$, $\text{TOF}_{\text{max}} = 30\text{--}160 \text{ h}^{-1}$). While these steric parameters appear to be the dominant factor for tailoring catalytic activity, the electronic factors allow for fine-tuning the activity, with trz systems outperforming the imi analogues (*cf* **5b** vs **5e**, and **5d** vs **5g**).

In order to probe the steric implications of the Cp* spectator ligand, different substrates with varying spatial requirement were evaluated, *viz.* butyraldehyde as a small substrate and *o*-tolualdehyde as a bulky substrate (Table 5, Fig. S56). Except for complexes **5a** and **6a** with methyl-substituted NHCs, catalytic activities increased when changing the substrate from 4-nitrobenzaldehyde to either of these two aldehydes (Table 5). In addition, turnover frequencies were generally higher for the bulkier *o*-tolualdehyde than for butyraldehyde. Interestingly, exchanging Cp for Cp* generally induced an improved catalytic activity towards both the relative to nitrobenzaldehyde smaller butyraldehyde and the sterically more demanding tolualdehyde (*cf* complexes **5b** and **6b**, $\text{TOF}_{\text{max}} = 70\text{--}80$ vs $160\text{--}180 \text{ h}^{-1}$; entries 2, 6, 8, 12). In both the Cp and Cp* analogues, the imidazolylidene ligand with the *i*Pr wingtip group (**5b** and **6b**) is favorable in the hydrosilylation catalysis over the methyl analogue (**5a** and **6a**; ($\text{TOF}_{\text{max}} = 10\text{--}20$ vs $70\text{--}80$ (**5a** vs **5b**), $6\text{--}20$ vs $160\text{--}180$ (**6a** vs **6b**, entries 1, 2, 5–8, 11, 12). These results suggest that the sterically

hindered catalysts with a Cp* spectator ligand do not discriminate bulkier substrates compared to their Cp analogues with a sterically better available iron centre. The choice of Cp vs Cp* is therefore substrate dependent and needs to be evaluated for determining the best performing catalyst system. As shown above for nitrobenzaldehyde, also for the butyraldehyde and tolualdehyde, the TOF_{max} correlates reasonably well with steric ligand parameters and much less with the ligand electronics (Fig. S57a,b), though again, the trz ligands outperform the imi series.

Table 5. Hydrosilylation of butyr- and tolualdehyde by iron(II) complexes **5** and **6**^a



entry	complex	substrate	conversion (%) ^b	yield (%) ^c	induction (min)	time (h)	TOF _{max} (h ⁻¹)
1	5a		100	79	80	24	20
2	5b		96	90	25	7	70
3	5e		100	99	10	1	240
4	5f		100	99	15	1.5	290
5	6a		56	45	80	45	6
6	6b		100	97	<20	1	160
7	5a		97	90	50	75	10
8	5b		100	93	20	3	80
9	5e		100	88	10	0.70	270
10	5f		100	99	25	1	360
11	6a		100	85	120	24	20
12	6b		100	99	20	2.3	180

^a General conditions: substrate (0.5 mmol), PhSiH₃ (0.6 mmol), [Fe] complex (5 μmol, 1 mol%); C₆Me₆ (50 μmol) as internal standard, DCE (2.5 mL), 60 °C. ^b Conversion determined by ¹H NMR spectroscopy as an average of at least two runs. ^c Spectroscopic yield determined for silylated butanol and deprotected 2-methyl-benzylalcohol, respectively.

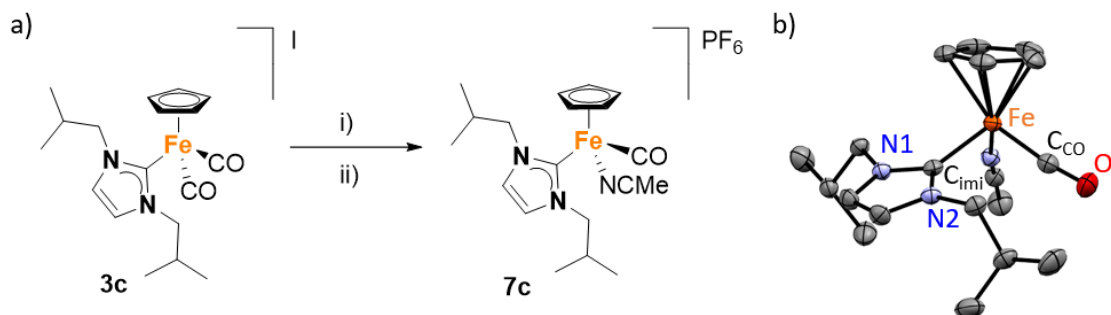
While there was no steric discrimination observed between tolualdehyde and butyraldehyde, a steric bias can be deduced, however, from experiments using very bulky substrates. Thus, neither mesityl benzaldehyde nor *o*-tolyl methylketone are converted even when using the most potent trz/Cp complex **5f**. Likewise, benzylacetate is not hydrosilylated under these conditions.

Mechanistic studies

While previous work disclosed a variety of mechanistically diverse catalytic cycles,^{27,46-50} we aimed here to shed some light on the mode of activation of these carbene iron catalysts in hydrosilylation. Therefore, a set of stoichiometric experiments was conducted as well as some tailored modifications of the catalyst precursor in order to facilitate the activation process. Considering the electronic saturation of the iron complexes **5** and **6** due to their 18 electron configuration, η^5 -to- η^3 Cp ring slippage⁵¹ or dissociation of an ancillary ligand constitute plausible activation pathways. The latter hypothesis is supported by earlier work that demonstrated that cationic complexes akin to **3** and **4** require UV irradiation to become active hydrosilylation catalysts.¹⁸

Probing iodide dissociation. When complex **5f** was dissolved in MeCN the colour gradually darkened and turned red within 10 min with concomitant formation of a second species according to ¹H NMR spectroscopy (Fig. S58). This change was reversible and was attributed to iodide dissociation and solvent coordination, a process that may be potentially relevant also for catalyst activation. To investigate the relevance of iodide coordination, complex **7c** was prepared in which the iodide was replaced with MeCN as a potentially better leaving group (Scheme 3). This complex was readily obtained from the dicarbonyl precursor **3c** via AgPF₆-mediated anion exchange

followed by UV irradiation in MeCN. Coordination of MeCN was confirmed by a characteristic singlet at $\delta_{\text{H}} = 2.28$ in the ^1H NMR spectrum (Fig. S46).



Scheme 3. Synthesis and ORTEP plot of complex **7c** (50% probability, all hydrogen atoms and non-coordinating PF_6^- anion omitted for clarity). Reagents and conditions: (i) AgPF_6 , CH_2Cl_2 , room temperature, 1 h; (ii) $h\nu$, MeCN, 1 h.

Complex **7c** catalysed the hydrosilylation of 4-nitrobenzaldehyde under standard conditions, though considerably slower than its iodide analogue **5c**. It required 70 h to reach 68% conversion compared to full conversion in 3 h with **5c** (Table S9). In an attempt to generate a putative catalytic iron alkoxide or iron hydride intermediate, complex **7c** was used as catalyst precursor in the presence of LiOiPr or NaBH_4 as additives.⁴⁹ Neither of these additives improved the catalytic activity and to the contrary, resulted in lower conversions. Also, stoichiometric ^1H NMR experiments did not lead to a defined complex and in the presence of LiOiPr only revealed broadening of the signals (Fig. S59). Likewise, addition of 0.6 eq. I_2 (relative to the iron complex) as a mild oxidizing agent to access a putative iron(III) species only lowered the catalytic performance. These data therefore point to some relevance of iodide coordination for imparting catalytic activity.

Monitoring stoichiometric experiments. Exposing complex **5f** to 2 eq. 4-nitrobenzaldehyde in CD₂Cl₂ at 60 °C for 30 min, induced the formation of a minor new set of aromatic signals at 8.10, 7.49 ppm of about 5% of the intensity compared to nitrobenzaldehyde (Fig. S60, S61). Addition of 4 eq. of PhSiH₃, led to complete consumption of 4-nitrobenzaldehyde within 10 min (Fig. S60c,d). When a stoichiometric mixture of 4-nitrobenzaldehyde and complex **5f** in DCE-*d*₄ was heated for 3 h an almost full depletion of the aldehyde signals was noted (Fig. S62).⁵² These changes may point to the formation of a paramagnetic species, such as an iron-alkoxy complex, though these events are clearly outside the catalytic time regime. Nonetheless, these data suggest that the substrate is interacting with the complex, but that the resulting species is either not stable enough to be isolated or not detectable by ¹H NMR spectroscopy. Notably, complex **5f** on its own is stable in refluxing CD₂Cl₂ for >2 h and degrades slowly in DCE-*d*₄, yet without the formation of any new signals (Fig. S63, S64).

Complementary reaction of complex **5f** with 3 eq. PhSiH₃ at 60 °C in the absence of aldehyde substrate induced spectral changes only after 20 min, with the appearance of a new set of signals and in particular a weak signal at -14.29 ppm (Fig. S65, S66) suggesting the formation of small quantities of an iron hydride species (<5%).^{53,54} The main species in the spectrum remained **5f** and this was visibly supported by the bright green colour of the solution. Addition of 2 eq. 4-nitrobenzaldehyde resulted in its full consumption within 10 minutes (Fig. S65c,d), and the disappearance of the hydride resonance. Upon addition of an extra 2 eq. aldehyde, again some 60% were consumed within 10 min (Fig. S65e), indicating full consumption of the silane and pointing to an iron species in solution that remains catalytically active. The presence of signals due to **5f** after these three turnovers revealed that only a small fraction of the precatalyst was transformed to the activate species. Notably, the iron complex in the presence of only PhSiH₃ was stable far

beyond the induction period typically observed in catalytic runs (up to 25 min for complex **5f** cf Tables 4 and 5, Fig. S67). Only extended incubation of **5f** at 60 °C led to a colour change from green to yellow with a 50% decrease of the signals of the original iron complex after 16 h (Fig. S67). Concomitantly, the ¹H NMR resonance of PhSiH₃ at 4.15 ppm decreased to ~5% and new singlets appeared at 5.02 and 5.19 ppm together with downfield shifted aromatic signals, which were attributed to reshuffled phenylsilane^{55,56} and siloxane species, the latter presumably formed due to fortuitous moisture or oxygen (Fig. S68).

The combined results from these NMR studies suggest the formation of a pre-equilibrium, either between the iron complex and the silane to form an iron hydride as the putative active species, or involving the iron complex and the aldehyde to form an iron substrate adduct. In either case, there is a strong preponderance towards the dissociated species, *i.e.* the starting materials. Notably, such a pre-equilibrium situation may rationalize the observed induction periods under catalytic conditions.

***In situ* reaction monitoring.** The CO functionalities in both the complex and the aldehyde substrate provided a diagnostic handle to use react-IR spectroscopy for investigating the catalyst activation and performance *in situ*. A catalytic run under standard conditions with complex **5f** revealed a gradual decrease of the C=O stretch vibration of the 4-nitrobenzaldehyde at 1711 cm⁻¹ and 1195 cm⁻¹, and a concomitant increase of a broad band at 1082 cm⁻¹ attributed to the C–O–Si unit indicative for the formation of the hydrosilylated products (Fig. 5). New phenylsilane products are suggested by the appearance of a broad band around $\nu_{\text{SiH}} = 2160 \text{ cm}^{-1}$.⁵⁷ Plotting the normalised

intensity changes over time yields similar rates as deduced from ^1H NMR monitoring of a parallel reaction (inset Fig. 5).

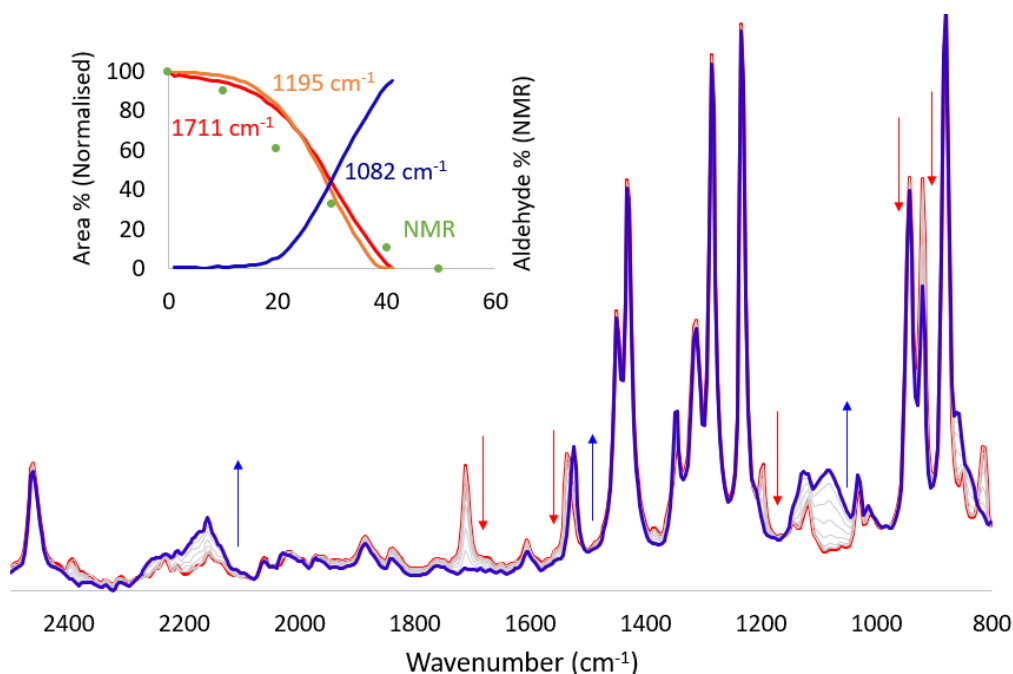


Figure 5. *In situ* FT-IR spectra recorded during hydrosilylation of 4-nitrobenzaldehyde with **5f** as catalyst under standard conditions (Table 4). Changes over time in 5 min intervals (red at 0 h and blue at 40 min), red arrows indicate change of signal intensities. Inset: Catalytic profile of two catalytic reactions, with conversions determined by ^1H NMR spectroscopy (green circles) and by IR spectroscopy from changes at 1195 and 1711 cm^{-1} (signals of 4-nitrobenzaldehyde, amber and red traces) and 1082 cm^{-1} (attributed to Si-O band in product, blue trace).

Catalyst activation was monitored in a set of stoichiometric experiments and corroborated the conclusions deduced from NMR spectroscopic analyses. Interaction of complexes **5c** or **5f** with 4-nitrobenzaldehyde in a 1:1 molar ratio resulted in a linear decrease of the carbonyl vibration bands of the complex and aldehyde at 1935 and 1711 cm^{-1} , respectively, and full disappearance within 40 min (Fig. S72, S73), strongly suggesting an interaction between the substrate and the catalyst

through CO dissociation from the iron coordination sphere.⁵⁸ A similar process has been established for the Shvo catalyst where CO dissociation is more favourable than η^5/η^3 ring slippage.^{59,60}

Stoichiometric experiments with complex **5f** and PhSiH₃ (1 eq.) showed substantially slower transformation of **5f** than in the presence of aldehyde under otherwise identical conditions (20% in 1 h; Fig. S75). Addition of 1 eq. of 4-nitrobenzaldehyde led to a full disappearance after 45 min of the CO band of the complex and full consumption of the substrate, together with almost 50% decrease of the phenylsilane. The time regime of these experiments suggests that the iron complex has a much higher affinity for the aldehyde and indicates that (reversible) CO dissociation and aldehyde coordination constitute a plausible catalyst activation pathway. Of course, the currently available data cannot rule out a Curtin-Hammett scenario with a catalytically irrelevant pre-equilibrium aldehyde coordination and parallel formation of an iron-hydride as active species present in too low quantities to be detected by react-IR. We note however that aldehyde coordination and conversion has a strong influence since earlier work in our group demonstrated that hydrosilylation of ketones is hampered unless the catalytically active species is formed through spiking of the reaction with some aldehyde.²⁷

In support of the mechanistic scenario involving ketone coordination in the catalyst activation step, an additional catalytic experiment was conducted in which complex **6b** was pre-stirred with 4-nitrobenzaldehyde for 1 h. Addition of PhSiH₃ initiated catalytic turnover immediately without any activation period and conversion was complete within 60 min according to ¹H NMR monitoring (Fig. S76). In comparison, without pre-stirring, an induction time of some 40 min was observed with this catalyst system, indicating that aldehyde coordination to iron is relevant. In contrast, pre-activation of complex **6b** with PhSiH₃ resulted in much slower conversion requiring

110 min to reach completion (Fig. S76). These data lend strong support to a catalyst activation involving CO ligand displacement by the aldehyde substrate rather than formation of an initial iron hydride species from the iron complex and the silane.

CONCLUSION

This work extends the diversity of piano-stool NHC iron complexes and includes variation of the NHC scaffold, the wingtip group, ancillary ligands, as well as modulation of the Cp ligand with the stronger donating Cp* analogue. Variability was also implemented on the synthetic level by introducing decarboxylation, so far unprecedented for iron(II) precursors, for preparing both imidazolylidene as well as triazolylidene piano-stool iron complexes. Application of these iron complexes with diverse ligand sets in the catalytic hydrosilylation of aldehydes revealed a clear trend in activity that depends strongly on the NHC scaffold ($\text{trz} > \text{imi}$) and revealed a good correlation with steric parameters as defined by the $\%V_{\text{bur}}$. Notably, the choice of Cp vs Cp* ligand may be substrate-dependent, for example the activity increase is opposite for nitrobenzaldehyde and butyraldehyde. Mechanistic investigations provide strong support for a catalyst activation that involves displacement of the CO ligand with the aldehyde substrate. Such a process rationalizes the critical role of the substrate in catalyst optimization and also the low activity of these complexes towards ketones. Moreover, it validates the need for a high modularity of the ligand sets in these piano-stool iron(II) complexes as demonstrated in this work. The option to vary virtually all parameters, from carbene scaffold to wingtip sterics and electronics, ancillary ligand, Cp substitution pattern, and counterions around the iron(II) center will also offer opportunities for exploring further catalytic applications beyond hydrosilylation.

EXPERIMENTAL SECTION

General Comments. Toluene, THF, CH₂Cl₂, Et₂O, and hexane were dried by passage through solvent purification columns. 1,2-Dichloroethane was dried over 4 Å molecular sieves and degassed with argon. All other reagents were commercially available and used without further purification. Metalation reactions and purification of complexes were carried out under an inert nitrogen atmosphere using standard Schlenk techniques. The synthesis of complexes **3a**, **3b**, **3d**, **3f**, **3g**, **5a**, **5b**, **5d**, **5f**, and **5g**,^{22,23,27} have been reported elsewhere, and the synthesis of all ligands is provided in the Supporting Information. NMR spectra were measured at 25 °C on Bruker spectrometers operating at 300 or 400 MHz (¹H NMR) and 75 or 101 MHz (¹³C{¹H} NMR), respectively. Chemical shifts (δ in ppm, coupling constants J in Hz) were referenced to residual solvent resonances downfield to SiMe₄. Assignments were made based on homo- and heteronuclear shift correlation spectroscopy. The purity of bulk samples of the complexes has been established by NMR spectroscopy and by elemental analysis, which was performed at the University of Bern Microanalytic Laboratory by using a Thermo Scientific Flash 2000 CHNS-O elemental analyser. High-resolution mass spectrometry was carried out with a Thermo Scientific LTQ Orbitrap XL instrument (ESI-TOF). IR spectra were recorded on a Jasco 4700 FT-IR instrument in CH₂Cl₂ solution at 1 cm⁻¹ resolution. Time-resolved online MCT FT-IR spectra were recorded on a ReactIR 15 Instrument (Mettler Toledo) equipped with a diamond probe (DiComp, optical range 3000–650 cm⁻¹). For online monitoring, the diamond probe was introduced into a 10 mL schlenk containing the reaction mixture and spectra were recorded at specific times. The experiments were run under nitrogen conditions. UV irradiation was carried out using a UVP Blak-Ray B-100AP lamp. Cyclic voltammetry measurements were carried out using a Metrohm Autolab Model PGSTAT101 potentiostat employing a gas-tight three-electrode cell under an argon atmosphere. A platinum disk with 7.0 mm² surface area was used as the working electrode and polished before each measurement. The reference electrode was Ag/AgCl; the counter electrode was Pt foil. Bu₄NPF₆ (0.1 M) in dry CH₂Cl₂ was used as supporting electrolyte with analyte concentrations of approximately 1 mM. The ferrocenium/ferrocene (Fc⁺/Fc) redox couple was used as an internal reference ($E_{1/2} = 0.50$ V vs SSCE).⁶¹

General Procedure for the Preparation of Complexes 3 and 4

Method A: The imidazolium/triazolium salt (1 equiv) and KO t Bu (1.2 equiv) were suspended in dry THF (10 mL). After 1 h of stirring at room temperature, the THF was removed under reduced pressure and the free carbene extracted in dry toluene (2 \times 6 mL) the resulting suspension was filtered into a dry toluene (3 mL) solution of [CpFe(CO) $_2$ I] or [Cp*Fe(CO) $_2$ I] (0.9 equiv). The resulting mixture was stirred at room temperature under exclusion of light for 16 h. The precipitate was collected by filtration, washed with toluene (2 \times 5 mL), extracted with CH $_2$ Cl $_2$, and dried in vacuo to yield the crude product as a light-sensitive material which hampered further purification.

Method B: The azolium carboxylate **2** and iron precursor were suspended in dry toluene (6 mL) and stirred at 80 °C for 16 h under exclusion of light. After cooling to room temperature, the precipitate was collected by filtration and purified as described in *Method A*.

Synthesis of 3a: According to *Method B* starting from **2a** (52 mg, 0.38 mmol) and [CpFe(CO) $_2$ I] (114 mg, 0.38 mmol) afforded complex **3a** as a yellow powder (65 mg, 43%). Analytical data agree with those reported for this compound.²³

Synthesis of 3c. According to *Method A* starting from **1c** (334 mg, 1.02 mmol), KO t Bu (155 mg, 1.28 mmol) and [CpFe(CO) $_2$ I] (259 mg, 0.85 mmol) afforded complex **3c** as a yellow powder (308 mg, 75%). Single crystals suitable for X-ray diffraction were obtained by slow diffusion of Et $_2$ O to a CH $_2$ Cl $_2$ solution of the complex.

1 H NMR (400 MHz, CD $_2$ Cl $_2$): δ 7.38 (br, 2H, H $_{Im}$), 5.31 (s, 5H, Cp), 4.00 (d, J = 7.8 Hz, CH $_2$), 2.22 (sept, J = 7.0 Hz, 2H, CH), 1.02 (d, J = 6.6 Hz, 12H, CH $_3$). 13 C { 1 H} NMR (101 MHz, CD $_2$ Cl $_2$): δ 211.81 (CO), 164.47 (C $_{Im-Fe}$), 125.54 (C $_{Im-H}$), 87.66 (Cp), 59.20 (CH $_2$), 29.66 (CH), 19.89 (CH $_3$). IR (CH $_2$ Cl $_2$, cm $^{-1}$): 2049, 2002 ν (CO). HRMS: m/z : calcd. for C $_{18}$ H $_{25}$ FeIN $_2$ O $_2$ [M – I] $^+$: 357.1246; found: 357.1260. Elemental Analysis calcd. (%) for C $_{18}$ H $_{25}$ FeIN $_2$ O $_2$ (484.16): C 44.65, H 5.20, N 5.79; found: C 44.34, H 5.15, N 5.69.

Synthesis of 3e: According to a slightly modified *Method A* from **1e** (157 mg, 0.53 mmol), KO t Bu (77 mg, 0.64 mmol). The mixture of base and ligand was directly cannulated into the toluene solution of [CpFe(CO) $_2$ I] (161 mg, 0.53 mmol). The solvents were removed under reduced pressure and the crude was used directly for the synthesis of **5e**. Single yellow crystals suitable for X-ray diffraction were obtained by slow diffusion of Et $_2$ O into a CH $_2$ Cl $_2$ solution of the complex.

^1H NMR (300 MHz, CD_2Cl_2): δ 5.31 (s, 5H, Cp), 5.11–5.02 (m, 1H, CH), 4.19 (s, 3H, NCH_3), 3.62–3.52 (m, 1H, CH), 1.62 (d, $J = 6$ Hz, 6H, CH_3), 1.43 (d, $J = 6$ Hz, 6H, CH_3). $^{13}\text{C}\{^1\text{H}\}$ NMR (101 MHz, CD_2Cl_2): δ 212.57 (CO), 152 ($\text{C}_{\text{trz}}\text{-Fe}$), 87.31 (Cp), 58.30 (NCH), 46.71 (C_{trz}), 39.85 (NCH_3), 27.58 (CCH), 23.90 (CH_3), 20.54 (CH_3). IR (CH_2Cl_2 , cm^{-1}): 2042, 1996 $\nu(\text{CO})$. HRMS: m/z : calcd. for $\text{C}_{16}\text{H}_{22}\text{FeIN}_2\text{O}$ [$\text{M} - \text{I}$] $^+$: 344.1056; found: 344.1050. Elemental Analysis calcd. (%) for $\text{C}_{16}\text{H}_{22}\text{FeIN}_3\text{O}_2$ (471.01): C 40.79, H 4.71, N 8.92; found: C 40.55, H 4.25, N 8.90.

Synthesis of 3f: According to *Method B* starting from **2f** (66 mg, 0.22 mmol) and $[\text{CpFe}(\text{CO})_2]\text{I}$ (77 mg, 0.25 mmol) afforded complex **3f** as a yellow powder (58 mg, 39%). Analytical data agree with those reported for this compound.²⁷

Synthesis of 4a: According to *Method A* starting from **2a** (45 mg, 0.32 mmol) and $[\text{Cp}^*\text{Fe}(\text{CO})_2]\text{I}$ (106 mg, 0.28 mmol). The crude product was extracted with CH_2Cl_2 and filtrated through a short pad of silica, the volatiles were removed by reduced pressure to yield the complex **4a** as a yellow powder (52 mg, 39%). Single crystals suitable for X-ray diffraction were obtained by slow diffusion of Et_2O to a CH_2Cl_2 solution of the complex.

^1H NMR (400 MHz, CD_2Cl_2) δ 7.42 (s, 2H, H_{Im}), 3.83 (s, 6H, NCH_3), 1.84 (s, 15H, $\text{Cp}^*\text{-CH}_3$). $^{13}\text{C}\{^1\text{H}\}$ NMR (101 MHz, CD_2Cl_2) δ 214.20 (CO), 172.90 ($\text{C}_{\text{Im}}\text{-Fe}$) 127.17 ($\text{C}_{\text{Im}}\text{-H}$), 99.45 ($\text{C}_{\text{Cp}^*\text{Ar}}$), 36.86 (NCH_3), 10.45 ($\text{Cp}^*\text{-CH}_3$). IR (CH_2Cl_2 , cm^{-1}): 2027, 1977 $\nu(\text{CO})$. HRMS: m/z : calcd. for $\text{C}_{17}\text{H}_{23}\text{FeIN}_2\text{O}_2$ [$\text{M} - \text{I}$] $^+$: 343.1103; found: 343.1106. Elemental Analysis calcd. (%) for $\text{C}_{17}\text{H}_{23}\text{FeIN}_2\text{O}_2$ (470.01): C 43.43, H 4.93, N 5.96; found: C 42.93, H 4.68, N 5.93.

Synthesis of 4b: According to *Method A* starting from **1b** (140 mg, 0.47 mmol), $\text{KO}t\text{Bu}$ (67 mg, 0.55 mmol) and $[\text{Cp}^*\text{Fe}(\text{CO})_2]\text{I}$ (160 mg, 0.43 mmol) afforded complex **4b** as a yellow powder (140 mg, 62%).

According to *Method B* starting from **2b** (75 mg, 0.38 mmol) and $[\text{Cp}^*\text{Fe}(\text{CO})_2]\text{I}$ (142 mg, 0.38 mmol) afforded complex **4b** as a yellow powder (141 mg, 71%). Single crystals suitable for X-ray diffraction were obtained by slow diffusion of Et_2O to a CH_2Cl_2 solution of the complex.

^1H NMR (CD_2Cl_2 , 400 MHz) δ 7.44 (s, 2H, Im), 4.53 (sept, $J = 7.0$ Hz, 2H, CH), 1.82 (s, 15H, $\text{Cp}^*\text{-CH}_3$), 1.61, 1.46 (d, $J = 6.1$ Hz, 12H, CH_3). $^{13}\text{C}\{^1\text{H}\}$ NMR (CD_2Cl_2 , 101 MHz): δ 214.03 (CO), 169.14 ($\text{C}_{\text{Im}}\text{-Fe}$), 122.59 ($\text{C}_{\text{Im}}\text{-H}$), 99.45 ($\text{C}_{\text{Cp}^*\text{Ar}}$), 55.15 (CH), 24.91, 24.47, 23.24 (CH_3), 10.24 ($\text{Cp}^*\text{-CH}_3$). IR (CH_2Cl_2 , cm^{-1}): 2024, 1977 $\nu(\text{CO})$. HRMS: m/z : calcd. for $\text{C}_{21}\text{H}_{31}\text{FeIN}_2\text{O}_2$

[M – I]⁺: 399.1729; found: 399.1731. Elemental Analysis calcd. (%) for C₂₁H₃₁FeIN₂O₂ (526.24): C 47.93; H 5.94; N 5.32 found: C 47.55, H 5.83, N 4.89.

General Procedure for the Preparation of Complexes 5 and 6

Complex **3** or **4** was dissolved in CH₂Cl₂ and irradiated with a high intensity UV lamp at 365 nm for 16 h. The resulting green solution was concentrated to ~2 mL and layered with dry hexane. After 24 h, the solution was filtered and evaporated to dryness to yield a dark green solid.

Synthesis of 5c: According to the general procedure from **3c** (308 mg, 0.64 mmol) afforded complex **5c** (189 mg, 64%). Single crystals suitable for X-ray diffraction were obtained by dissolving the crude in CH₂Cl₂ (2 mL) and layering with dry hexanes.

¹H NMR (300 MHz, CD₂Cl₂, –20 °C): δ 7.20, 7.06 (br, 2H, H_{Im}), 4.90 (dd, *J* = 13.7, 8.9 Hz, 1H, CH₂), 4.43 (s, 5H, Cp–H), 4.34 (dd, *J* = 13.6, 7.1 Hz, 1H, CH₂), 4.19–4.01 (m, 2H, CH₂), 2.39–2.21 (m, 1H, CH), 2.10–2.03 (m, 1H, CH), 1.06 (d, *J* = 6.6 Hz, 3H, CH₃), 1.00 (dd, *J* = 11.9, 6.8 Hz, 6H, CH₃), 0.74 (d, *J* = 6.6 Hz, 3H, CH₃). ¹³C{¹H} NMR (101 MHz, CD₂Cl₂): δ 224.50 (CO), 184.14 (C_{Im}–Fe), 122.77 (C_{Im}–H), 80.30 (C_{Cp}), 60.68, 58.39 (NCH₂), 29.51, 29.25 (CH), 19.95, 19.87, 19.72, 19.56 (CH₃). IR (CH₂Cl₂, cm^{–1}): 1934 ν(CO). HRMS: *m/z*: calcd. for C₁₇H₂₅FeIN₂O [M – I]⁺: 329.1304; found: 329.1311. Elemental Analysis calcd. (%) for C₁₇H₂₅FeIN₂O (456.15): C 44.76, H 5.52, N 6.14; found: C 44.58, H 5.37, N 6.25.

Synthesis of 5e: The general procedure starting from **3e** afforded complex **5e** (50 mg, 21%, overall yield from **1e**). Single crystals suitable for X-ray diffraction were obtained by dissolving the crude in CH₂Cl₂ (2 mL) and layering with dry hexanes.

¹H NMR (400 MHz, d-toluene, 65 °C): δ 6.42–6.08, 4.52–4.27 (broad, 2H, CH) 4.20 (s, 5H, Cp), 3.11 (s, CH₃), 1.53–1.35, 1.08–0.99, 0.95–0.83 (broad, 12H, CH₃). Major Rotamer (60%): ¹H NMR (400 MHz, CD₂Cl₂, –25 °C): δ 6.36 (sept, 6.7 Hz, 1H, NCH), 3.96 (sept, 7.3 Hz, 1H, CH), 4.39 (s, 5H, Cp), 4.01 (s, CH₃), 1.65, 1.49–1.45 (d, 6.7 Hz, 6H, NCCH₃) 1.38, 1.17 (d, 7.3 Hz, 6H, CH₃). ¹³C{¹H} NMR (101 CD₂Cl₂, –25 °C): 225.07 (CO), 163.57 (C_{trz}–Fe), 151.25 (C_{trz}–C) 79.94 (Cp), 57.89 (NCH) 38.19 (NCH₃), 26.84 (CCH), 24.25, 23.32, 20.39, 20.03 (CH₃). Minor rotamer

(40%): ^1H NMR (400 MHz, CD_2Cl_2 , $-25\text{ }^\circ\text{C}$): δ 5.40 (sept, 6.7 Hz, 1H, NCH), 4.71 (sept, 7.3 Hz, 1H, CH), 4.40 (s, 5H, Cp), 4.03 (s, CH_3), 1.55, 1.35 (d, 6.7 Hz, 6H, NCCH_3) 1.49–1.45, 1.27 (d, 7.3 Hz, 6H, CH_3). $^{13}\text{C}\{^1\text{H}\}$ NMR (101 CD_2Cl_2 , $-25\text{ }^\circ\text{C}$): 225.17 (CO), 164.52 ($\text{C}_{\text{trz}}\text{-Fe}$), 153.60 ($\text{C}_{\text{trz}}\text{-C}$) 80.24 (Cp), 56.17 (NCH) 38.29 (NCH_3), 28.21 (CCH), 23.45, 23.30, 20.37, 19.99 (CH_3). IR (CH_2Cl_2 , cm^{-1}): 1928 $\nu(\text{CO})$. HRMS: m/z : calcd. for $\text{C}_{15}\text{H}_{22}\text{FeN}_3\text{O}$ [$\text{M} - \text{I}$] $^+$: 316.1107; found: 316.1099. Elemental Analysis calcd. (%) $\text{C}_{15}\text{H}_{22}\text{FeN}_3\text{O}$ (456.15): C 40.66, H 5.00, N 9.48; found: C 41.16, H 5.10, N 9.52.

Synthesis of 6a: The imidazolium carboxylate **2a** (72 mg, 0.51 mmol) and $[\text{Cp}^*\text{Fe}(\text{CO})_2]\text{I}$ (267 mg, 0.70 mmol) were suspended in dry toluene (5 mL) and stirred at $80\text{ }^\circ\text{C}$ for 16 h under exclusion of light. After cooling to room temperature, the precipitate was collected by filtration, washed with toluene (2×3 mL). According to the general procedure complex **6a** was afforded as a green powder (39.4 mg, 40%). Single crystals suitable for X-ray diffraction were obtained by dissolving the product in CH_2Cl_2 (2 mL) and layering with dry hexanes.

^1H NMR (400 MHz, CD_2Cl_2) δ 7.08, 6.98 (d, $J = 4.0$ Hz, 2H, H_{im}), 4.04, 3.86 (s, 6H, NCH_3), 1.69 (s, 15H, $\text{Cp}^*\text{-CH}_3$). $^{13}\text{C}\{^1\text{H}\}$ NMR (101 MHz, CD_2Cl_2) δ 226.66 (CO), 191.15 ($\text{C}_{\text{im}}\text{-Fe}$) 124.69, 124.47 ($\text{C}_{\text{im}}\text{-H}$), 89.51 ($\text{C}_{\text{Cp}^*\text{Ar}}$), 43.08 (NCH_3), 39.27 (NCH_3), 10.65 ($\text{Cp}^*\text{-CH}_3$). IR (CH_2Cl_2 , cm^{-1}): 1914 $\nu(\text{CO})$. HRMS: m/z : calcd. for $\text{C}_{16}\text{H}_{23}\text{FeIN}_2\text{O}$ [$\text{M} - \text{I}$] $^+$: 315.1155; found: 315.1154. Elemental Analysis calcd. (%) for $\text{C}_{16}\text{H}_{23}\text{FeIN}_2\text{O}$ (442.12) (Et_2O) 0.2%: C 44.16, H 5.51, N 6.13; found: C 43.81, H 6.05, N 6.27.

Synthesis of 6b: According to the general procedure from **4b** (140 mg, 0.27 mmol) afforded complex **6b** as a green powder (80 mg, 60%). Single crystals suitable for X-ray diffraction were obtained by dissolving the product in CH_2Cl_2 (2 mL) and layering with dry hexanes.

^1H NMR δ 7.17, 7.07 (d, $J = 4.0$ Hz, 2H, Im), 5.63 – 5.42, 5.25–4.97 (m, 2H, CH), 1.66 (s, 15H, $\text{Cp}^*\text{-CH}_3$), 1.62, 1.48, 1.42, 1.38 (d, $J = 6.4$ Hz, 12H, CH_3). $^{13}\text{C}\{^1\text{H}\}$ NMR (101 MHz, CD_2Cl_2) δ 119.90, 119.35 ($\text{C}_{\text{im}}\text{-H}$), 88.99 ($\text{C}_{\text{Cp}^*\text{Ar}}$), 53 (CH), 24.89, 24.87, 23.35 (CH_3), 10.89 ($\text{Cp}^*\text{-CH}_3$). IR (CH_2Cl_2 , cm^{-1}): 1910 $\nu(\text{CO})$. HRMS: m/z : calcd. for $\text{C}_{20}\text{H}_{31}\text{FeIN}_2\text{O}$ [$\text{M} - \text{I}$] $^+$: 371.1780; found: 371.1775. Elemental Analysis calcd. (%) for $\text{C}_{20}\text{H}_{31}\text{FeIN}_2\text{O}$ (498.08): C 48.21; H 6.27; N 5.62; found: C 48.25; H 6.30; N 6.07

Synthesis of 7c: The imidazolium salt **1c** (334 mg, 1.02 mmol) and KO^tBu (155 mg, 1.28 mmol) were suspended in dry THF (10 mL). After 1 h of stirring at room temperature, the mixture was added to a suspension of [CpFe(CO)₂]I (159 mg, 0.85 mmol) in dry toluene (30 mL) and stirred at room temperature for 1 h under exclusion of light. The precipitate was collected by filtration, washed with ether (2 × 10 mL) taken up in CH₂Cl₂ and filtrated through a short pad of silica. All volatiles were removed under reduced pressure. The residue was dissolved in CH₂Cl₂ and AgPF₆ (212 mg, 0.84 mmol) was added. After 1 h of stirring at room temperature under exclusion of light, the mixture was filtrated through a short pad of silica and the solvents were removed under reduced pressure. The residue was dissolved in MeCN (15 mL) and irradiated with a high intensity UV lamp at 365 nm for 40 h. The volatiles were removed under reduced pressure. Single crystals suitable for X-ray diffraction were obtained by dissolving the product in CH₂Cl₂ and layering with dry hexanes (202 mg, 47%).

¹H NMR (400 MHz, CD₂Cl₂): δ 7.29 (s, 2H, H_{Im}), 4.71 (s, 5H, Cp), 4.16–4.11 (m, 2H, CH₂), 3.96–3.91 (m, 2H, CH₂), 2.28 (s, 3H, CH₃CN), 2.18 (m, 2H, CH), 1.02, 0.96 (d, *J* = 6.6 Hz, 12H, CH₃). ¹³C{¹H} NMR (101 MHz, CD₂Cl₂): δ 220.05 (CO), 176.56 (C_{Im}-Fe), 134.61 (CNCH₃) 124.24 (C_{Im}-H), 82.59 (Cp), 58.43 (CH₂), 29.73 (CH), 20.02 (CH₃), 5.16 (CH₃CN). IR (CH₂Cl₂, cm⁻¹): 1980 ν(CO). HRMS: *m/z*: calcd. for C₁₉H₂₈FeN₃O [M - PF₆]⁺: 370.1576; found: 370.1575. Elemental Analysis calcd. (%) for C₁₉H₂₈F₆FeN₃OP (515.26): C 44.29, H 5.48, N 8.16; found: C 44.33, H 5.66, N 8.11.

Typical Procedure for Hydrosilylation Catalysis.

A solution of 4-nitrobenzaldehyde (0.5 mmol), phenylsilane (74 μL; 0.6 mmol), and hexamethylbenzene (8.1 mg; 0.05 mmol) or 1,3,5-trimethoxybenzene (8.4 mg; 0.05 mmol) in 1,2-dichloroethane (2.0 mL) was stirred at 60 °C for 10 min under an N₂ atmosphere. The iron complex was added from a stock solution (0.5 mL, 0.01 M, 5 μmol), and aliquots were taken at specific times, diluted with CDCl₃, and analysed by ¹H NMR spectroscopy.

Crystallographic Details.

All measurements were made on an Oxford Diffraction SuperNova area-detector diffractometer⁶² using mirror optics monochromated Mo Kα radiation (λ = 0.71073 Å) and Al filtering.⁶³ The unit

cell constants and an orientation matrix for data collection were obtained from a least-squares refinement of the setting angles of reflections in the range $2.0^\circ < \theta < 27.9^\circ$. A total of 728 frames were collected using ω scans, with 8+8 seconds exposure time, a rotation angle of 1.0° per frame, a crystal-detector distance of 65.0 mm, at $T = 173(2)$ K. Data reduction was performed using the CrysAlisPro⁶² program. The intensities were corrected for Lorentz and polarization effects, and a numerical absorption correction based on gaussian integration over a multifaceted crystal model was applied. Data collection and refinement parameters are presented in the Supporting Information. The structure was solved by direct methods using SHELXT⁶⁴, which revealed the positions of the non-hydrogen atoms of the title compound. All non-hydrogen atoms were refined anisotropically. All H-atoms were placed in geometrically calculated positions and refined using a riding model where each H-atom was assigned a fixed isotropic displacement parameter with a value equal to 1.2Ueq of its parent atom (1.5Ueq for methyl groups). Refinement of the structure was carried out on F^2 using full-matrix least-squares procedures, which minimized the function $\Sigma w(F_o2 - F_c2)^2$. The weighting scheme was based on counting statistics and included a factor to downweight the intense reflections. All calculations were performed using the SHELXL-2014/7⁶⁵ program in OLEX2.⁶⁶ Further crystallographic details are compiled in Tables S2–S6 in the Supporting Information. Crystallographic data for the structures of all compounds reported in this paper have been deposited with the Cambridge Crystallographic Data Centre (CCDC) as supplementary publication numbers 2072827 (**3c**), 2072824 (**3e**), 2072829 (**4a**), 2072831 (**4b**), 2072826 (**5c**), 2072828 (**5e**), 2072825 (**6a**), 2072832 (**6b**), 2072830 (**7c**).

SUPPORTING INFORMATION

Experimental procedures for ligands, NMR spectra, free energy calculations, cyclic voltammetry, crystallographic details, buried volume calculations, catalytic and mechanistic details.

ACKNOWLEDGMENT

We thank the European Research Council (ERC 615653) for generous financial support of our work in this area and the group of Chemical Crystallography of the University of Bern for X-ray analyses.

The authors declare no competing financial interest

REFERENCES

- (1) Bauer, I.; Knölker, H. J. Iron Catalysis in Organic Synthesis. *Chem. Rev.* **2015**, *115*, 3170–3387. <https://doi.org/10.1021/cr500425u>.
- (2) Bolm, C.; Legros, J.; Le Pailh, J.; Zani, L. Iron-Catalyzed Reactions in Organic Synthesis. *Chem. Rev.* **2004**, *104*, 6217–6254. <https://doi.org/10.1021/cr040664h>.
- (3) Morris, R. H. Asymmetric Hydrogenation, Transfer Hydrogenation and Hydrosilylation of Ketones Catalyzed by Iron Complexes. *Chem. Soc. Rev.* **2009**, *38*, 2282–2291. <https://doi.org/10.1039/b806837m>.
- (4) Zhang, M.; Zhang, A. Iron-Catalyzed Hydrosilylation Reactions. *Appl. Organomet. Chem.* **2010**, *24*, 751–757. <https://doi.org/10.1002/aoc.1701>.
- (5) Du, X.; Huang, Z. Advances in Base-Metal-Catalyzed Alkene Hydrosilylation. *ACS Catal.* **2017**, *7*, 1227–1243. <https://doi.org/10.1021/acscatal.6b02990>.
- (6) Lopes, R.; Royo, B. Iron N-Heterocyclic Carbenes in Reduction Reactions. *Isr. J. Chem.* **2017**, *57*, 1151–1159. <https://doi.org/10.1002/ijch.201700055>.
- (7) Wei, D.; Darcel, C. Iron Catalysis in Reduction and Hydrometalation Reactions. *Chem. Rev.* **2019**, *119*, 2550–2610. <https://doi.org/10.1021/acs.chemrev.8b00372>.
- (8) Raya-Barón, Á.; Oña-Burgos, P.; Fernández, I. Iron-Catalyzed Homogeneous Hydrosilylation of Ketones and Aldehydes: Advances and Mechanistic Perspective. *ACS Catal.* **2019**, *9*, 5400–5417. <https://doi.org/10.1021/acscatal.9b00201>.
- (9) Yun, J.; Kim, D.; Yun, H. A New Alternative to Stryker's Reagent in Hydrosilylation: Synthesis, Structure, and Reactivity of a Well-Defined Carbene–Copper(II) Acetate

- Complex. *Chem. Commun.* **2005**, 942, 5181. <https://doi.org/10.1039/b509964a>.
- (10) Lopes, R.; Pereira, M. M.; Royo, B. Selective Reduction of Nitroarenes with Silanes Catalyzed by Nickel N-Heterocyclic Carbene Complexes. *ChemCatChem* **2017**, 9, 3073–3077. <https://doi.org/10.1002/cctc.201700218>.
- (11) Hofmann, R. J.; Vlatkovic, M.; Wiesbrock, F. Fifty Years of Hydrosilylation in Polymer Science: A Review of Current Trends of Low-Cost Transition-Metal and Metal-Free Catalysts, Non-Thermally Triggered Hydrosilylation Reactions, and Industrial Applications. *Polymers*. **2017**, 9, 534. <https://doi.org/10.3390/polym9100534>.
- (12) Bart, S. C.; Lobkovsky, E.; Chirik, P. J. Preparation and Molecular and Electronic Structures of Iron(0) Dinitrogen and Silane Complexes and Their Application to Catalytic Hydrogenation and Hydrosilation. *J. Am. Chem. Soc.* **2004**, 126, 13794–13807. <https://doi.org/10.1021/ja046753t>.
- (13) Wu, J. Y.; Stanzl, B. N.; Ritter, T. A Strategy for the Synthesis of Well-Defined Iron Catalysts and Application to Regioselective Diene Hydrosilylation. *J. Am. Chem. Soc.* **2010**, 132, 13214–13216. <https://doi.org/10.1021/ja106853y>.
- (14) Sanagawa, A.; Nagashima, H. Cobalt(0) and Iron(0) Isocyanides as Catalysts for Alkene Hydrosilylation with Hydrosiloxanes. *Organometallics* **2018**, 37, 2859–2871. <https://doi.org/10.1021/acs.organomet.8b00389>.
- (15) Hu, M. Y.; He, Q.; Fan, S. J.; Wang, Z. C.; Liu, L. Y.; Mu, Y. J.; Peng, Q.; Zhu, S. F. Ligands with 1,10-Phenanthroline Scaffold for Highly Regioselective Iron-Catalyzed Alkene Hydrosilylation. *Nat. Commun.* **2018**, 9, 1–12. <https://doi.org/10.1038/s41467-017-02472-6>.
- (16) Zhang, M.; Zhang, J.; Ni, X.; Shen, Z. Bis(Phenolate) N-Heterocyclic Carbene Rare Earth

- Metal Complexes: Synthesis, Characterization and Applications in the Polymerization of n-Hexyl Isocyanate. *RSC Adv.* **2015**, *5*, 83295–83303. <https://doi.org/10.1039/c5ra16447h>.
- (17) Kandepi, V. V. K. M.; Cardoso, J. M. S.; Peris, E.; Royo, B. Iron(II) Complexes Bearing Chelating Cyclopentadienyl-N-Heterocyclic Carbene Ligands as Catalysts for Hydrosilylation and Hydrogen Transfer Reactions. *Organometallics* **2010**, *29*, 2777–2782. <https://doi.org/10.1021/om100246j>.
- (18) Jiang, F.; Bézier, D.; Sortais, J. B.; Darcel, C. N-Heterocyclic Carbene Piano-Stool Iron Complexes as Efficient Catalysts for Hydrosilylation of Carbonyl Derivatives. *Adv. Synth. Catal.* **2011**, *353*, 239–244. <https://doi.org/10.1002/adsc.201000781>.
- (19) Bézier, D.; Jiang, F.; Roisnel, T.; Sortais, J. B.; Darcel, C. Cyclopentadienyl-NHC Iron Complexes for Solvent-Free Catalytic Hydrosilylation of Aldehydes and Ketones. *Eur. J. Inorg. Chem.* **2012**, *2*, 1333–1337. <https://doi.org/10.1002/ejic.201100762>.
- (20) Demir, S.; Gökçe, Y.; Kaloğlu, N.; Sortais, J. B.; Darcel, C.; Özdemir, I. Synthesis of New Iron-NHC Complexes as Catalysts for Hydrosilylation Reactions. *Appl. Organomet. Chem.* **2013**, *27*, 459–464. <https://doi.org/10.1002/aoc.3006>.
- (21) Lopes, R.; Cardoso, J. M. S.; Postigo, L.; Royo, B. Reduction of Ketones with Silanes Catalysed by a Cyclopentadienyl- Functionalised N-Heterocyclic Iron Complex. *Catal. Letters* **2013**, *143*, 1061–1066. <https://doi.org/10.1007/s10562-013-1081-8>.
- (22) Buchgraber, P.; Toupet, L.; Guerchais, V. Syntheses, Properties, and X-Ray Crystal Structures of Piano-Stool Iron Complexes Bearing an N-Heterocyclic Carbene Ligand. *Organometallics* **2003**, *22*, 5144–5147. <https://doi.org/10.1021/om034056o>.
- (23) Mercs, L.; Labat, G.; Neels, A.; Ehlers, A.; Albrecht, M. Piano-Stool Iron(II) Complexes as Probes for the Bonding of N-Heterocyclic Carbenes: Indications for π -Acceptor Ability.

- Organometallics* **2006**, *25*, 5648–5656. <https://doi.org/10.1021/om060637c>.
- (24) Guisado-Barrios, G.; Bouffard, J.; Donnadieu, B.; Bertrand, G. Crystalline 1H-1,2,3-Triazol-5-Ylidenes: New Stable Mesoionic Carbenes (MICs). *Angew. Chemie - Int. Ed.* **2010**, *49*, 4759–4762. <https://doi.org/10.1002/anie.201001864>.
- (25) Bouffard, J.; Keitz, B. K.; Tonner, R.; Guisado-Barrios, G.; Frenking, G.; Grubbs, R. H.; Bertrand, G. Synthesis of Highly Stable 1,3-Diaryl-1 H -1,2,3-Triazol-5-Ylidenes and Their Applications in Ruthenium-Catalyzed Olefin Metathesis. *Organometallics* **2011**, *30*, 2617–2627. <https://doi.org/10.1021/om200272m>.
- (26) Trnka, T. M.; Morgan, J. P.; Sanford, M. S.; Wilhelm, T. E.; Scholl, M.; Choi, T. L.; Ding, S.; Day, M. W.; Grubbs, R. H. Synthesis and Activity of Ruthenium Alkylidene Complexes Coordinated with Phosphine and N-Heterocyclic Carbene Ligands. *J. Am. Chem. Soc.* **2003**, *125*, 2546–2558. <https://doi.org/10.1021/ja021146w>.
- (27) Johnson, C.; Albrecht, M. Triazolylidene Iron(II) Piano-Stool Complexes: Synthesis and Catalytic Hydrosilylation of Carbonyl Compounds. *Organometallics* **2017**, *36*, 2902–2913. <https://doi.org/10.1021/acs.organomet.7b00349>.
- (28) Ohki, Y.; Hatanaka, T.; Tatsumi, K. C - H Bond Activation of Heteroarenes Mediated by a Half-Sandwich Iron Complex of N-Heterocyclic Carbene. **2008**, No. 7, 17174–17186. <https://doi.org/10.1021/ja8063028>.
- (29) Liang, Q.; Osten, K. M.; Song, D. Iron-Catalyzed Gem-Specific Dimerization of Terminal Alkynes. *Angew. Chemie - Int. Ed.* **2017**, *56*, 6317–6320. <https://doi.org/10.1002/anie.201700904>.
- (30) Liang, Q.; Sheng, K.; Salmon, A.; Zhou, V. Y.; Song, D. Active Iron(II) Catalysts toward Gem-Specific Dimerization of Terminal Alkynes. *ACS Catal.* **2019**, *9*, 810–818.

<https://doi.org/10.1021/acscatal.8b03552>.

- (31) Liang, Q.; Hayashi, K.; Rabeda, K.; Jimenez-Santiago, J. L.; Song, D. Piano-Stool Iron Complexes as Precatalysts for Gem-Specific Dimerization of Terminal Alkynes. *Organometallics* **2020**, *39*, 2320–2326. <https://doi.org/10.1021/acs.organomet.0c00271>.
- (32) Riener, K.; Haslinger, S.; Raba, A.; Högerl, M. P.; Cokoja, M.; Herrmann, W. A.; Kühn, F. E. Chemistry of Iron N-Heterocyclic Carbene Complexes: Syntheses, Structures, Reactivities, and Catalytic Applications. *Chem. Rev.* **2014**, *114*, 5215–5272. <https://doi.org/10.1021/cr4006439>.
- (33) Royo, B. *Cyclopentadienyl-Functionalized n-Heterocyclic Carbene Complexes of Iron and Nickel: Catalysts for Reductions*, in: *Advances in Organometallic Chemistry and Catalysis*; Pombiero, Armando, J., L., Ed.; John Wiley & Sons Inc., 2014. [https://doi.org/10.1016/s1351-4180\(14\)70389-7](https://doi.org/10.1016/s1351-4180(14)70389-7).
- (34) Johnson, C.; Albrecht, M. Piano-Stool N-Heterocyclic Carbene Iron Complexes: Synthesis, Reactivity and Catalytic Applications. *Coord. Chem. Rev.* **2017**, *352*, 1–14. <https://doi.org/10.1016/j.ccr.2017.08.027>.
- (35) Voutchkova, A. M.; Appelhans, L. N.; Chianese, A. R.; Crabtree, R. H. Disubstituted Imidazolium-2-Carboxylates as Efficient Precursors to N-Heterocyclic Carbene Complexes of Rh, Ru, Ir, and Pd. *J. Am. Chem. Soc.* **2005**, *127*, 17624–17625. <https://doi.org/10.1021/ja056625k>.
- (36) Wyer, E.; Gucciardo, G.; Leigh, V.; Müller-Bunz, H.; Albrecht, M. Comparison of Carbene and Imidazole Bonding to a Copper(I) Center. *J. Organomet. Chem.* **2011**, *696*, 2882–2885. <https://doi.org/10.1016/j.jorganchem.2011.02.012>.
- (37) Albrecht, M.; Maji, P.; Häusl, C.; Monney, A.; Müller-Bunz, H. N-Heterocyclic Carbene

- Bonding to Cobalt Porphyrin Complexes. *Inorganica Chim. Acta* **2012**, *380*, 90–95.
<https://doi.org/10.1016/j.ica.2011.08.039>.
- (38) Ségaud, N.; McMaster, J.; Van Koten, G.; Albrecht, M. Imidazolylidene Cu(II) Complexes: Synthesis Using Imidazolium Carboxylate Precursors and Structure Rearrangement Pathways. *Inorg. Chem.* **2019**, *58*, 16047–16058.
<https://doi.org/10.1021/acs.inorgchem.9b02568>.
- (39) Shapovalov, S. S.; Tikhonova, O. G.; Skabitskii, I. V.; Kolos, A. V.; Sakharov, S. G.; Torubaev, Y. V. Oxidation of Iron Complex with NHC Ligand with Molecular Iodine. *Russ. J. Inorg. Chem.* **2019**, *64*, 1418–1423. <https://doi.org/10.1134/S0036023619110184>.
- (40) Shapovalov, S. S.; Tikhonova, O. G.; Grigor'eva, M. O.; Skabitskii, I. V.; Simonenko, N. P. Metal Complexes with the N-Heterocyclic Ligand: Synthesis, Structures, and Thermal Decomposition. *Russ. J. Coord. Chem. Khimiya* **2019**, *45*, 706–711.
<https://doi.org/10.1134/S1070328419100063>.
- (41) Naumann, S.; Schmidt, F. G.; Schowner, R.; Frey, W.; Buchmeiser, M. R. Polymerization of Methyl Methacrylate by Latent Pre-Catalysts Based on CO₂-Protected N-Heterocyclic Carbenes. *Polym. Chem.* **2013**, *4*, 2731. <https://doi.org/10.1039/c3py00073g>.
- (42) Akita, M.; Terada, M.; Tanaka, M.; Morooka, Y. Some Additional Aspects of Versatile Starting Compounds for Cationic Organoiron Complexes: Molecular Structure of the Aqua Complex [(H₅-C₅Me₄Et)Fe(CO)₂(OH₂)]BF₄ and Solution Behavior of the THF Complex [(H₅-C₅R₅)Fe(CO)₂(THF)]BF₄. *J. Organomet. Chem.* **1996**, *510*, 255–261.
[https://doi.org/http://dx.doi.org/10.1016/0022-328X\(95\)05918-F](https://doi.org/http://dx.doi.org/10.1016/0022-328X(95)05918-F).
- (43) Günther, H. *NMR-Spektroskopie*; Georg Thieme Verlag Stuttgart, 1973.
- (44) Mathew, P.; Neels, A.; Albrecht, M. 1,2,3-Triazolylidenes as Versatile Abnormal Carbene

- Ligands for Late Transition Metals. *J. Am. Chem. Soc.* **2008**, No. 130, 13534–13535.
- (45) Falivene, L.; Cao, Z.; Petta, A.; Serra, L.; Poater, A.; Oliva, R.; Scarano, V.; Cavallo, L. Towards the Online Computer-Aided Design of Catalytic Pockets. *Nat. Chem.* **2019**, *11*, 872–879. <https://doi.org/10.1038/s41557-019-0319-5>.
- (46) Gutsulyak, D. V.; Kuzmina, L. G.; Howard, J. A. K.; Vyboishchikov, S. F.; Nikonov, G. I. Cp(Pri₂MeP)FeH₂SiR₃: Nonclassical Iron Silyl Dihydride. *J. Am. Chem. Soc.* **2008**, *130*, 3732–3733. <https://doi.org/10.1021/ja800983n>.
- (47) Lam, Y. C.; Nielsen, R. J.; Goddard, W. A.; Dash, A. K. The Mechanism for Catalytic Hydrosilylation by Bis(Imino)Pyridine Iron Olefin Complexes Supported by Broken Symmetry Density Functional Theory. *Dalt. Trans.* **2017**, *46*, 12507–12515. <https://doi.org/10.1039/c7dt02300f>.
- (48) Smith, P. W.; Dong, Y.; Tilley, T. D. Efficient and Selective Alkene Hydrosilylation Promoted by Weak, Double Si-H Activation at an Iron Center. *Chem. Sci.* **2020**, *11*, 7070–7075. <https://doi.org/10.1039/d0sc01749c>.
- (49) Bleith, T.; Gade, L. H. Mechanism of the Iron(II)-Catalyzed Hydrosilylation of Ketones: Activation of Iron Carboxylate Precatalysts and Reaction Pathways of the Active Catalyst. *J. Am. Chem. Soc.* **2016**, *138*, 4972–4983. <https://doi.org/10.1021/jacs.6b02173>.
- (50) Metsänen, T. T.; Gallego, D.; Szilvási, T.; Driess, M.; Oestreich, M. Peripheral Mechanism of a Carbonyl Hydrosilylation Catalysed by an SiNSi Iron Pincer Complex. *Chem. Sci.* **2015**, *6*, 7143–7149. <https://doi.org/10.1039/c5sc02855h>.
- (51) Connor, J. M.; Casey, C. P. Ring-Slippage Chemistry of Transition-Metal Cyclopentadienyl and Indenyl Complexes. *Chem. Rev.* **1987**, *87*, 307–318. <https://doi.org/10.1021/cr00078a002>.

- (52) No Product Was Observed by ¹H NMR and nor Any Precipitation Was Observed. No precipitation was observed in the NMR tube nor any new signals, indicative of a product formation.
- (53) Hamon, J.-R.; Hamon, P.; Toupet, L.; Costuas, K.; Saillard, J.-Y. Classical and Non-Classical Iron Hydrides: Synthesis, NMR Characterisation, Theoretical Investigation and X-Ray Crystal Structure of the Iron(IV) Dihydride $[\text{Cp}^*\text{Fe}(\text{Dppe})(\text{H})_2]^+ \text{BF}_4^-$. *Comptes Rendus Chim.* **2002**, *5*, 89–98. [https://doi.org/10.1016/s1631-0748\(02\)01327-9](https://doi.org/10.1016/s1631-0748(02)01327-9).
- (54) Li, H.; Misal Castro, L. C.; Zheng, J.; Roisnel, T.; Dorcet, V.; Sortais, J. B.; Darcel, C. Selective Reduction of Esters to Aldehydes under the Catalysis of Well-Defined NHC-Iron Complexes. *Angew. Chemie - Int. Ed.* **2013**, *52*, 8045–8049. <https://doi.org/10.1002/anie.201303003>.
- (55) Becker, B.; Corriu, R. J. P.; Guérin, C.; Henner, B. J. L. Hypervalent Silicon Hydrides: Evidence for Their Intermediacy in the Exchange Reactions of Di- and Tri-Hydrogenosilanes Catalysed by Hydrides (NaH, KH and LiAlH₄). *J. Organomet. Chem.* **1989**, *369*, 147–154. [https://doi.org/10.1016/0022-328X\(89\)88002-7](https://doi.org/10.1016/0022-328X(89)88002-7).
- (56) Docherty, J. H.; Dominey, A. P.; Thomas, S. P. Nucleophile Induced Ligand Rearrangement Reactions of Alkoxy- and Arylsilanes. *Tetrahedron* **2019**, *75*, 3330–3335. <https://doi.org/10.1016/j.tet.2019.04.062>.
- (57) Bellamy, L. J. *The Infra-Red Spectra of Complex Molecules*, 3rd ed.; Chapman and Hall Ltd.: London, 1975.
- (58) Analysis of This Reaction Mixture by ¹H NMR Spectroscopy Revealed the Same Changes in Chemical Shifts as Observed by ¹H NMR Spectroscopic Reaction Monitoring (Fig. S74, Cf Fig. S63).

- (59) Warner, M. C.; Verho, O.; Bäckvall, J. E. CO Dissociation Mechanism in Racemization of Alcohols by a Cyclopentadienyl Ruthenium Dicarbonyl Catalyst. *J. Am. Chem. Soc.* **2011**, *133*, 2820–2823. <https://doi.org/10.1021/ja1098066>.
- (60) Stewart, B.; Nyhlen, J.; Martín-Matute, B.; Bäckvall, J. E.; Privalov, T. A Computational Study of the CO Dissociation in Cyclopentadienyl Ruthenium Complexes Relevant to the Racemization of Alcohols. *Dalt. Trans.* **2013**, *42*, 927–934. <https://doi.org/10.1039/c2dt31919e>.
- (61) Connelly, N. G.; Geiger, W. E. Chemical Redox Agents for Organometallic Chemistry. *Chem. Rev.* **1996**, *96*, 877–910. <https://doi.org/10.1021/cr940053x>.
- (62) Diffraction, O. Oxford Diffraction (2018). CrysAlisPro (Version 1.171.40.39a). Oxford Diffraction Ltd., Yarnton Oxfordshire, UK. 2018, pp 279–288.
- (63) Macchi, P.; Bu, H.; Chimpri, A. S. Research Papers Low-Energy Contamination of Mo Microsource X-Ray Radiation : Analysis and Solution of the Problem Research Papers. *J. Appl. Crystallogr.* **2011**, *44*, 763–771. <https://doi.org/10.1107/S0021889811016232>.
- (64) Sheldrick, G. M. Research Papers SHELXT – Integrated Space-Group and Crystal-Structure Determination Research Papers. *Acta Crystallogr. Sect. A* **2015**, 3–8. <https://doi.org/10.1107/S2053273314026370>.
- (65) Sheldrick, G. M. Crystal Structure Refinement with SHELXL. *Acta Crystallogr. Sect. C* **2015**, 3–8. <https://doi.org/10.1107/S2053229614024218>.
- (66) Dolomanov, O. V; Bourhis, L. J.; Gildea, R. J.; Howard, J. A. K.; Puschmann, H. OLEX2 : A Complete Structure Solution , Refinement and Analysis Program. *J. Appl. Crystallogr.* **2009**, *42*, 2008–2010. <https://doi.org/10.1107/S0021889808042726>.